A FINAL REPORT
ON THE NASA GRANT NAG-1-1612 OF

LARGE-VORTEX CAPTURE BY A WING AT VERY HIGH ANGLES OF ATTACK

Submitted to

Mr. Williams Sellers, Branch Head
Dr. Roland Juslin, Technical Monitor

Flow Modeling and Control Branch
MS 197
NASA Langley Research Center
Hampton, VA 23665-5225

Prepared by

J.M. Wu and **J.Z. Wu**

Co-Investigators:
G.A. Denny and **X.Y. Lu**
The University of Tennessee Space Institute
Tullahoma, TN 37388-8897

July, 1996

1. Introduction

In generating the lift on a wing, the static stall is a severe barrier. As the angle of attack, α, increases to the stall angle, α_{stall}, the flow separation point on the upper surface of the wing moves to the leading edge, so that on a two-dimensional airfoil or a large-aspect-ratio wing, the lift abruptly drops to a very low level. Therefore, the first generation of aeronautical flow type, i.e., the *attached steady flow*, has been limited to $\alpha < \alpha_{stall}$.

Owing to the obvious importance in applications, therefore, a great effort has been made in the past two decades to enlarge the range of usable angles of attack by various flow controls for a large-aspect-ratio wing. Basically, relevant works fall into two categories. The first category is usually refereed to as *separation control*, which concentrates on partially separated flow at $\alpha < \alpha_{stall}$. Since the first experimental study of Collins and Zelenevitz (1975), there has been ample literature showing that a partially separated flow can be turned to almost *fully attached* by flow controls, so that the lift is recovered and the stall is delayed (for a recent work see Seifert et al. 1993). It has been well established that, in this category, unsteady controls are much more effective than steady ones and can be realized at a very low power-input level (Wu et al. 1991; Seifert et al. 1993).

The second and more ambitious category of relevant efforts is the *post-stall lift enhancement*. Its possibility roots at the existence of a second lift peak at a very high angle of attack. In fact, As α further increases from α_{stall}, the completely separated flow develops and gradually becomes a *bluff-body flow*. This flow gives a normal force to the airfoil with a lift component, which reaches a peak at a maximum utilizable angle of attack, $\alpha_m \simeq 40°$. This second peak is of the same level as the first lift peak at α_{stall}. Meanwhile, the drag is also quickly increased (e.g., Fage and Johansen 1927; Critzos et al. 1955). Figure 1 shows a typical experimental lift and drag coefficients of NACA-0012 airfoil in this whole range of angle of attack.

Obviously, without overcoming the lift crisis at α_{stall}, the second lift peak is completely useless. Thus, the ultimate goal of post-stall lift enhancement is to fill the lift valley after stall by flow controls, so that a wing and/or flap can work at the whole range of $0° < \alpha < \alpha_m$. Relevant early experimental studies have been extensively reviewed by Wu et al. (1991), who concluded that, first, similar to the leading-edge vortex on a slender wing, the lift enhancement on a large-aspect-ratio wing should be the result of capturing a vortex on the upper surface of the wing; and, second, using steady controls cannot reach the goal, and one must rely on unsteady controls with low-level power input as well. Wu et al. (1991) also conjectured that the underlying physics of post-stall lift enhancement by unsteady controls consists of a chain of mechanisms: *vortex layer instability - receptivity - resonance - nonlinear streaming*.

Experimental studies by Hsiao's group (Hsiao et al. 1990, 1993, 1994; Chang et al. 1992) using a NACA 63_3-018 airfoil, and Zhou and Fernholz (Zhou et al. 1993) using a NACA-0025 airfoil (with sharp edge forward), confirmed the above basic ideas. In a range of post-stall angle of attack till about 35°, a local unsteady excitation (acoustic and/or oscillating flap) near leading edge may increase the lift by 40 % to 70 %, and the lift/drag ratio can be increased up to 80% at a moderate α. The possibility of capturing a vortex by unsteady control was also confirmed analytically by Chernyshenko (1995). He used a simple theoretical model to prove that while a vortex above a circular cylinder in an oncoming flow is unstable and must run away, it can be stabilized and captured in the mean sense by a two-point alternative blowing-suction.

In spite of these positive progresses, a full understanding of the wing flow at a post-stall angle of attack and its control is still lacking due to the well-known complexity of such flows. Shear layers shed from both leading and trailing edges of the wing, rolling up into mutually interacting vortices. The secondary and tertiary separations from the mid portion of upper surface may also be induced. All these make the flow field inherently unsteady, and no such a simple theory as the classic linear aerodynamics for steady attached flow is possible. Therefore, a full clarification of the mechanisms of post-stall lift enhancement by unsteady controls is highly desired, which heavily relies on careful numerical simulations and detailed experimental flow-field surveys.

Motivated by the above need and supported by NASA Langley Research Center under the Grant NAG-1-1612 (1994-1996), we carried out a series of two-dimensional Navier-Stokes computation of a post-stall turbulent flow over an airfoil and its unsteady control. The purpose of the study was twofold: to reproduce computationally the lift-drag characteristics of uncontrolled and controlled flows, and using the detailed flow-field data base to further clarify the physical mechanisms therein. The results will be outlined in the next section. They confirmed the above experimental discovery qualitatively, and did lead to a deeper physical understanding.

These recent experimental and computational progresses open a new avenue to pass through the barrier of static stall of classic wings, so that a wing or a flap with proper built-in unsteady control devices could enjoy a sufficient lift well beyond the stall till a much higher angle of attack. We believe that, after some further study, this post-stall flow control technique can be applied to the industrial designs within a few years. In particular, it can be immediately used to increase the function of a flap system in landing, so that a reduction of its size and an increase of its working angle of attack are possible.

This report consists of the following contents. Section 2 discusses the basic physics relevant to the project. In Section 3 we present our numerical approach, and in Section 4, the results and discussion. Some brief concluding remarks are made in Section 5.

2. Physical Background of Post-Stall Flow Control

We first discuss the basic physical mechanisms behind the post-stall flow control, which provided a guidance to our computation.

2.1. The Vortical Source of Post-Stall Lift and Drag

It is well known that, at least at low Mach numbers, the lift (and drag) on a wing is entirely from the generated vorticity in asymmetric boundary layers on the upper and lower surfaces of the wing through the viscosity and no-slip condition. Recently, Wu and Wu (1996) re-emphasized this vortical source of aerodynamic force by explicitly putting the Kutta-Joukowski lift formula (a counterclockwise circulation Γ is assumed positive)

$$L = -\rho U \Gamma \tag{1}$$

and its three-dimensional extension on the basis of *viscous rotational flow theory*. Wu and Wu show that these formulas hold if the flow is incompressible and steady, and if the Reynolds number approaches infinity (i.e., the *Euler limit* of Navier-Stokes flow).

For high Reynolds-number attached flow, the circulation Γ in (1) is well predicted by classic potential-flow theory. In contrast, in a fully separated unsteady flow which is our concern, although the favorable circulation in upper-surface boundary layer is mostly lost, Eq. (1) should still hold in a time-averaged sense if the mean Γ of the whole flow field can be properly estimated. This is however not an easy task. In the Kirchhoff-Rayleigh theory (Lamb 1932, §77), the circulation in (1) already exists implicitly, because the free streamlines shed from the leading and trailing edges of an inclined flat plate are nothing but vortex sheets, or the Euler limit of shear layers. This pair of vortex sheets are of the same strength but the upper one is longer, and hence a net lift. But, the theory assumes that the lee-side pressure takes the undisturbed value, which results in an underestimate of the normal force. Roshko (1954a,b) showed that the Kirchhoff-Rayleigh theory can be modified to fit well the flat-plate experimental result of Fage and Johansen (1927), if the lee-side pressure is reduced to a more negative value by introducing a single empirically determined constant. Similar result was obtained by Wick (1954). The physical implication of this empirical correction to the Kirchhoff-Rayleigh theory can be made clear from the following observation.

In Kirchhoff's theory, the free streamlines or vortex sheets do not roll into concentrated vortices. In reality, however, the Kirchhoff flow is impossible under the Euler limit. Once the airfoil starts to move at a post-stall angle of attack, the separated vortex sheets must immediately roll up at their ends, which is essentially the most common mechanism of the quick formation of concentrated vortices in a fluid of small viscosity (Betz 1950). Thus, the vortex sheets can never have a chance to extend to infinity as assumed in Kirchhoff's theory. After the vortex sheets roll into concentrated vortices, they must carry more circulation above a wing than open sheets (Wu and Wu 1992), and produce a higher normal force than

that predicted by the Kirchhoff-Rayleigh theory. In other words, the difference between Kirchhoff and Rayleigh's theoretical prediction and experimental value of the normal force is a measure of the net contribution of vortex-sheet rolling up.

It is of interest to notice that, without appealing to any separated-flow model, a simple-minded consideration can already capture most part of the experimental lift and drag of Fig. 1. Assume the oncoming flow with momentum ρU directly hits the airfoil of chord length c such that, to satisfy the no-through condition on the wall, its entire normal momentum is transferred to the normal force N acted on the airfoil at a rate U. This gives

$$N \simeq K \rho U^2 c \sin \alpha,$$

where the proportional coefficient K can be fixed as 1.2 based on the flat-plate experiment of Fage and Johansen (1927). Thus, the lift and drag coefficients are estimated by

$$C_l \simeq 1.2 \sin 2\alpha, \quad C_d \simeq 2.4 \sin^2 \alpha, \qquad (2a,b)$$

as also plotted in Fig. 1. The agreement with experiment is surprisingly good in most part of post-stall angles of attack; the main deviation in both C_l and C_d occurring only in the regime of attached flow. Obviously, from the aerodynamic-efficiency point of view, the optimal use of vortical force is in this regime of attached flow, where C_d is so low that one can enjoy a very high lift/drag ratio of $O(10^2)$. On the other hand, the fitting of Eq. (2a,b) with experimental data indicates that they may roughly cover the contribution of rolled-up vortices, including the streaming effect. Due to the simple trigonometry relation between lift and drag, the lift/drag ratio for fully separated flow at high α inevitably reduces to $O(1)$. Note that the peak C_l of the airfoil ($\simeq 1.15$) is slightly overestimated by taking $K = 1.2$, and this geometry-dependent difference could be due to the fact that a shear layer shed from a sharp edge (as in the flat-plate case) will form a stronger vortex than that from a smooth surface, as is well known on slender wings. This was also why in the experiment of Zhou and Fernholz (Zhou at al. 1993) the airfoil was reversely installed.

```
Figure 1 here
```

From the above simple observation, one may already learn something important in the post-stall flow control. First, one should enhance the rolling up of leading-edge shear layer (Wu and Wu 1992), such that its total length (and circulation) above the wing is even larger than the attached boundary layer. This implies that the control should promote the discretization of this layer into individual vortices, and their merging. If possible, the leading edge should be made sharp.

Second, since kinematically the total circulation (including that carried away by wake vortices) in the flow field must be zero, the formation of unfavorable trailing vortex is

inevitable. But, what one could do through control is to suppress the rolling up of trailing-edge shear layer and/or push the trailing vortex downstream.

2.2. Unforced Randomness vs Forced Resonance in Separated Flow

We now examine the specific dominating mechanisms involved in the post-stall flow control. Obviously, two major mechanisms must play an essential role in a fully separated flow field: the *local instability* of separated shear layers from both leading and trailing edges, and the *global instability* that causes vortex shedding. While our understanding of controlling the former can be greatly benefited from the studies of forced mixing-layers (e.g., Ho and Huerre 1984), that of the latter is benefited from the studies of forced cylinder-wake flows (e.g., Rockwell 1990).

2.2.1. Unforced Separated Flow

The dimensionless shear-layer frequency is defined as

$$St_{\text{shear}} = \frac{f_{\text{shear}}\theta}{\overline{U}}, \quad \overline{U} = \frac{1}{2}(U_1 + U_2), \tag{3}$$

where θ is the momentum thickness of the layer and U_1 and U_2 the velocities at its two edges. An unforced straight shear layer is unstable if $0 \leq St_{\text{shear}} \leq 0.08$ (Ho and Hurre 1984). For different U_1 and U_2, the most unstable mode always occurs when $St_{\text{shear}} \simeq 0.032$ if the flow is laminar, see Fig. 2; and $St_{\text{shear}} \simeq 0.044$ - 0.048 if the flow is turbulent (Ho and Huerre, *ibid*). This most unstable frequency is referred to as the *natural frequency* and denoted by f^0_{shear}. Note that since θ is a increasing function of the streamwise distance from the separation point, say s; hence, f^0_{shear} must be a decreasing function of s.

Figure 2 here

On the other hand, the global instability that causes vortex shedding is the result of a sufficiently large zone of *absolute instability* (e.g., Huerre and Monkewitz 1990), which, once occurs, implies that perturbations will propagate both upstream and downstream. Therefore, owing to the coexistence of a variable f^0_{shear} and a natural shedding frequency f^0_{shed} between the leading shear layer and trailing vortices, plus the fluctuating frequencies of secondary and tertiary separations, the unforced separated flow must be a *multi-frequency system*, in which the shear-layer evolution and vortex shedding process are already coupled with and modulate each other. Because three frequencies that are not mutually integer times of each other imply chaos, the random behavior of unforced separated flow is inevitable.

2.2.2. Forced Shear Layer

As is well known, for a forced shear layer, the key parameter is the forcing frequency f_e. The *response frequency* of the shear layer, f^r_{shear}, may differ from f^0_{shear} but is shifted to a subharmornic of f_e. Under this f^r_{shear}, the shear layer rolls into discrete vortices, which then merge into larger ones with the characteristic frequency correspondingly reduced. This process will promote the merging and enhance the entrainment. Such a *subharmonic resonance* and *frequency lock-in* are known to be the basic mechanism for effective shear-layer control, which always leads to a more regularized flow field than non-resonant case.

In addition, a forcing at very low frequency of $O(10^{-1} f^0_{shear})$ and a finite amplitude may cause the so-called "collective interaction" (Ho and Nosseir 1981; Ho and Huang 1982) or "forced fusion" (Rockwell 1972), in which a coalescence of many small vortices into a large one occurs within a short distance. Unal and Rockwell (1988) have proposed that this mechanism be responsible to the vortex formation from separated shear layers in a bluff-body flow. This could also be especially valuable for our purpose, because the length scale of a fully separated flow is usually not large enough for the formation of a large lifting vortex merely from successive pairings. On the other hand, unlike the straight shear layer appearing in the experiments of Ho et al. and Rockwell, above an airfoil the leading shear layer has a natural tendency to turn down and roll up. This makes the multi-vortex coalescence easier to occur under proper control. Because there is no absolute distinction between a perturbed shear layer and its discrete version, in what follows we shall call this phenomenon the *rolling-up coalescence*.

2.2.3. Forced Vortex Shedding and Unsteady Control

After the controlled leading-edge shear layer is quickly discretized and a strong lifting vortex is formed by merging, the lifting vortex will interact with trailing vortices just like a bluff-body flow. Here we also have the frequency lock-in phenomenon, where the natural shedding frequency shifts to a harmonic of f_e (e.g., Stansby 1976). It is therefore possible to find a proper range of f_e so that *the leading and trailing vortices are both effectively modulated by a single forcing.* Moreover, since disturbances can propagate both upstream and downstream in absolutely unstable zone, we have a natural mechanism to close the loop of resonance. In such a resonant flow the unfavorable random modes are suppressed, making the retained main modes very *regular* and *strong*.

From the above discussions it is clear that, unlike the wake control of a circular-cylinder flow, say, we now have to pay more attention to the flow field above the airfoil. In particular, the focus must be on the control of leading-edge shear layer. Its upstream location and high receptivity, as well as the fact that it is the only source of lift, make the leading-edge shear layer the most effective constituent to control. Correspondingly, in post-stall lift enhancement the imposed control must be *asymmetric* relative to the airfoil configuration, as seen from the above-mentioned experiments with a single leading-edge

control device. In this way, not only the enhancement of a time-averaged normal force (which is the drag in bluff-body flows with symmetric geometry and forcing), but also that of a time-averaged lift, can be achieved.

2.3. Other Factors in Unsteady Control

Except for frequency, some other factors may affect the resonance and flow patterns.

2.3.1. Forcing Amplitude

Under an upper bound, the increase of amplitude of forcing has a positive effect on the increase of lift. In particular, if the lifting vortex is to be formed through the "rolling-up coalescence" of small vortices, a sufficient amplitude is necessary to shift the small vortices away from their mean position. The amplitude is easily controlled either experimentally (Chang et al. 1992) or numerically. The forcing amplitude should be optimized from a compromise between the desired lift increase and the power input.

2.3.2. Phase Velocity

For two modes to be in a resonant state, in addition to the frequency condition (subharmonic), their phase velocity must be the same, which is difficult to control. Fortunately, as seen from Fig. 3, for the shear layer this naturally happens when St_{shear} defined by (3) is between 0.032 and 0.08. Thus, a forcing at $St_{shear} = 0.04$ will cause a resonance with the mode of $St_{shear} = 0.08$.

```
Figure 3 here
```

2.3.3. Phase Angle

Ho and Huerre (1984) remarked that the phase angle, say β, of the basic and subharmonic modes also has important influence on the vortex-pairing process. The best case is $\beta = 0$, and the worst one is $\beta = \pi$: the latter will reduce the subharmonic growth rate by 30%. To ensure the mode interaction be in phase needs a *local close-loop control*, which could be achieved only by using *micro-sensors* and *micro-actuators*. Note that the phase problem is more complicated on a wing than a simple mixing layer — the former involves the phase of vortex shedding process as well. Note that if the rolling-up coalescence is to be promoted, the detailed evolution of leading-edge shear layer, including its frequency, phase velocity, and phase angle, become immaterial (Ho and Nossier 1981). A reduction of relevant factors is therefore possible, and the control problem is simplified.

2.3.4. Wing Configuration

The airfoil configuration certainly has a crucial effect on the unforced and forced flow pattern. Wu and Wu (1992) stressed that most design criteria of the common airfoils to

be used in attached-flow regime is no longer meaningful. As mentioned before, a sharp leading edge may produce a stronger favorable vortex. In addition, since a sharp edge fixes the separation point, it is expected that such an edge will ensure a good spanwise correlation, very important in three-dimensional flow control. Then, the shape of upper surface determines whether the captured vortex can move comfortably, and whether the secondary separation can be easily alleviated. Moreover, if the length scale of the airfoil can match the wave length of discrete vortices, better control effect could be expected. Finally, some unusual trailing-edge shape could be invented to alleviate the unfavorable influence of trailing vortices.

2.3.5. Reynolds Number

The Reynolds number based on chord length (Re_c) or the cross-flow length scale of the body (Re_d for a cylinder; $Re_{cross} = Re_c \sin \alpha$ for an airfoil) has a significant effect on the transition position, and hence also on vortex shedding frequency, base pressure, and force coefficient (Roshko 1961; Jones et al. 1969; Güven et al. 1980; Oertel 1990; Williamson 1996). For a cylinder flow, as Re_d increases, several distinct regimes exist as shown in Fig. 4 (Williamson 1996). In the figure, A - J denote different regimes, from laminar steady flow regime to boundary-layer transition regime. Our concern is mainly in the regimes E - J (critical, supercritical, and post-critical regimes). In the E - H range, due to the delay of turbulent separation and narrowing of turbulent wake, there is a sharp drop of base suction and drag. This behavior indicates that great care must also be taken for the post-stall airfoil flow in these Reynolds numbers.

```
Figure 4 here
```

In particular, the narrowing of turbulent wake may result in attached turbulent wake vortices without shedding, at least in the mean sense. Because our control means is designed for generically unsteady flow with vortex shedding, in the critical regime of airfoil flow the unsteady control may not be necessary or effective.

Unfortunately, in contrast to the cylinder flow, it is very difficult to determine the quantitative dependence of the post-stall airfoil-flow pattern on the Reynolds number. Here the airfoil geometry and angle of attack must also be involved. For example, from practical point of view, Re_c should be no less than 2×10^6 (Wlezien 1996, private communication). At $\alpha = 25°$, say, this gives $Re_{cross} = 8.5 \times 10^5$, which may just fall into the critical regime. Rumsey et al. (1987) have found asymptotically steady numerical solution for a turbulent flow over NACA-0012 airfoil at $\alpha = 25°$ and $Re_c = 1.3 \times 10^6$ ($Re_{cross} = 0.55 \times 10^5$). A systematic exploration of the dependence of post-stall flow pattern on the Reynolds number should be one of the key issues in our future study.

3. Numerical Method

Our numerical study has confirmed many of the above physical observations. The method and results are presented in this and next sections. Due to the limitation of budget and computer resources, some important factors affecting the control has not studied and should be pursued in the future.

3.1. Numerical Scheme

A compressible Navier-Stokes solver, VNS, was adapted to the present problem. The scheme is approximate factorized, using second-order central differencing in space plus a fourth-order artificial viscosity, and is of second-order implicit in time. The code has been confirmed to work well at low Mach numbers by several test cases, including stationary and oscillating airfoil flows, as well as flow over circular cylinder with vortex shedding. An O-grid was used with 141×181 (circumferencial $\times$ normal) meshes. The grid was stretched such that the mesh height adjacent to the wall is less than 10^{-4}. The computational domain has a radius of 12 chord length, which was proved sufficient by numerical tests.

To check the resolution, a denser grid was used to compute a typical case for both unforced and forced flows. The result was almost the same as the 141×181 grid, the only difference being the detailed phase of chaotic force fluctuation. Thus, the grid-size independence of the computation was confirmed.

As stated before, Re_c should be no less than 2×10^6. The computational resource available to us does not allow for a direct numerical simulation or large-eddy simulation; thus, a Raynolds-average with some turbulence model is necessary. The choice of turbulence model has very strong effect on the numerical results. In a computation of dynamic stall, a comparative study of an algebraic model (Baldwin and Lomax 1978), an one-equation model (Spalart and Allmaras 1992), and the k-ϵ model has been made by Ko and McCroskey (1995), who concluded that the Spalart-Allmaras model seems to be the best. Various near-wall damping functions were compared by Patel et al. (1985). Because detailed benchmark experimental data are not available for the range of angles of attack we are studying, it is difficult to decide the model effect. For simplicity, the Baldwin-Lomax model was used, along with the Launder-Sharma (1974) wall-damping function. The B-L model is known to overestimate the lift for separated flow (Ko and McCroskey 1995), which was also observed in our computation.

The computation would be much more complicated if it is to faithfully simulate an oscillating flap, where a moving grid has to be imbedded in a fixed global grid. Such a computation is being undertaken and will be reported elsewhere. In the present study we used a local periodic blowing-suction at 2.5% chord length from the leading edge, to mimic the effect of forcing. This location has been shown by the experiments of Hsiao et al. (cited in § 1) to be most effective over a wide range of angle of attack.

The adherence condition on airfoil surface is imposed except a few grid points in the blowing-suction location. A non-reflectional condition (Thompson 1990) is imposed on the outer boundary of the computational domain. The initial condition is simply taken as a uniform flow. After starting, the transient state evolves to a quasi-periodic state. All the data were drawn after the quasi-periodic state was reached.

3.2. Parameters

In the experiments of Hsiao's group (see the references cited before), it was reported that the forcing frequency was chosen as the shear-layer frequency f^0_{shear} for lower post-stall α, and the natural shedding frequency f^0_{shed} for higher α. However, because θ and $\overline{U}$ vary along a streamline, and because above an airfoil the separated shear layer is no longer straight and there can be secondary and tertiary separations, the natural frequency f^0_{shear} can hardly be identified (Hsiao et al. did not explain how the shear-layer frequency was detected). If f^0_{shear} was referred to the initial frequency at separation point, it could not be the best choice. In contrast, in the experiment of Zhou and Fernhotz (Zhou et al. 1993) it was found that the optimal effect occurred when f_e was the first and second superharmonics of f_{shed}. Because the natural vortex-shedding frequency can be accurately determined by computation or experiment, it is much more convenient to use f^0_{shed} as a reference in choosing our f_e. We thus define a relative forcing frequency

$$\widehat{f}_e = \frac{f_e}{f^0_{shed}}, \tag{4}$$

and for most runs we chose

$$\widehat{f}_e = 2^j, \quad j = 0, \pm 1, \pm 2, ..., \tag{5}$$

such that the imposed f_e can effectively modulate the vortex shedding process. As addressed before, due to the same variable feature of f^0_{shear}, in a range of angles of attack it is possible that $\widehat{f}_e$ given by (5) also falls into a proper range that can promote the vortex discretization in the shear layer or their merging.

The choice of Reynolds number was more complex. On one hand, as discussed in § 2.3.5, we need to work on as high Re_c as possible but avoiding the critical regime. On the other hand, as Re_c increases, more small-scale vortices will appear, so that the flow will tend to be more chaotic and take more time to reach a quasi-periodic state. Our preliminary numerical tests confirmed this trend. To save computer time, therefore, we chose $Re_c = 5 \times 10^5$, i.e., $Re_{cross} = 2.1 \times 10^5$. This is of the same order as those in the experimental studies cited above (up to 6.7×10^5, Zhou et al. 1993) and in the computation of Ko and McCroskey (1995), which was 6×10^5. Note that a circular-cylinder flow at this Re is in subcritical regime.

The Mach number was fixed at 0.2. Along with $Re_c = 5 \times 10^5$, this implies that the computed airfoil model has a chord length $c = 11$ cm (a larger Mach number implies a smaller c).

The airfoil for computation was NACA 0012, since its uncontrolled force character over the whole range of $0° \leq \alpha \leq 360°$ has been extensively studied by careful experiments (Critzos et al. 1955; Fig. 1 above). But, this is certainly not the optimal shape for post-stall control purpose.

The periodic blowing-suction was simulated over five grid points of total length l to form a velocity profile $v(s)$. The flow rate, defined by

$$c_\mu = \frac{|v|_{\max} l}{U c \sin \alpha}, \tag{6}$$

is fixed to 2.5%, which at $\alpha = 25°$ corresponds to $|v|_{\max}/U \simeq 0.42$. Introducing the factor $\sin \alpha$ is to ensure that with the same c_μ a higher α requires a larger $|v|_{\max}/U$ as it should be. Tests case at $\alpha = 25°$ showed that below $c_\mu = 1.0\%$ the forcing effect is almost negligible. It should be stressed that, the required c_μ may well be reduced by using a smaller l (for that case a denser grid would be needed) while keeping the same $|v|_{\max}$. We believe that it is not the nominal c_μ but *maximum disturbance velocity*, $|v|_{\max}/U$, that is crucial for the control (Chang et al. 1992).

The computation was carried out on a Cray-C90 supercomputer. Each run took about $1 \sim 2$ hours of CPU time. In the computation, the angle of attack was taken at $18°$, $20°$, $25°$, $30°$, and $35°$. Based on (3), a selective set of values of forcing frequency, $\hat{f}_e = 0.0, 0.5, 1.0, 2.0$, and 4.0, was first tested at $\alpha = 25°$. Then the most effective values of f_e were tested for other α. The output data include: instantaneous C_l, C_d and associated power spectra; their time average; instantaneous and time-averaged vorticity contours; the time-averaged pressure distribution and streamlines.

4. Results and Discussion

We now present the resulting change of forces and flow patterns due to forcing. We concentrate on the lift and drag first, which is the essential data to justify the feasibility of the post-stall flow control technique.

4.1. Effect of Forcing Frequency

We look at the effect of forcing frequency, with fixed $\alpha = 25°$. In this case we found that

$$f^0_{\text{shed}} = 0.152 f^0_{\text{shear}},$$

where f^0_{shear} is estimated at a point right downstream of the separation point.

Figure 5a gives a typical time variation of lift and drag coefficients for the unforced flow. The corresponding power spectrum of C_l is shown in fig. 5b, where the only peak

is at St_{shed}, all other modes being not excited. A quasi-periodicity is clearly seen, mainly modulated by the natural vortex shedding frequency. We define

$$St_{\text{shed}} = \frac{f_{\text{shed}} c \sin \alpha}{U}, \tag{7}$$

which for $\alpha = 25°$ was found to be 0.158. The time-averaged lift and drag coefficients are 1.017 and 0.543, respectively, both are higher than the classic experimental values 0.84 and 0.36 at the same Reynolds number (Critzos et al. 1955; Fig. 1). As mentioned before, this discrepancy is due mainly to the use of algebraic turbulence model. Thus, the results are of value mainly in the relative sense.

```
┌─────────────────────────────────────┐
│            Figure 5 here            │
└─────────────────────────────────────┘
```

The time-dependent C_l and C_d under forcing, as well as their power spectra, are shown in Figs. 6 through 9. The time-averaged lift and drag are compared in Table 1, where the amplitudes of C_l and C_d, in terms of root-square mean, are also listed. The following effects of forcing frequency are then evident.

```
┌─────────────────────────────────────┐
│           Figures 6 - 9 here        │
└─────────────────────────────────────┘
```

First, the *harmonic resonance with vortex shedding* obviously happens at $\widehat{f_e} = 1.0$ and 2.0. In both cases many harmonic modes of f^0_{shed} are excited. Consequently, we obtain the most favorable increase of lift/drag ratio (49.2% and 46.7%, respectively). In particular, the random high-frequency modes observed for unforced case are almost completely suppressed when $f_e = 2f^0_{\text{shed}}$, implying a *perfect frequency lock-in*, which is the characteristics of strongest resonance. This pattern must represent a well-organized vortical flow.

Second, the above two cases have very different amplitudes of C_l and C_d. While at $\widehat{f_e} = 1.0$ the amplitude is even larger than the unforced case, it is much smaller at $\widehat{f_e} = 2.0$. Figures 4a and 5a suggest that a dramatic change of the vortex shedding pattern takes place as the forcing frequency is doubled: one large vortex is broken into two smaller ones, which shed off at $2f_e$. Therefore, a resonant state is not necessarily associated with amplitude amplification. The same phenomenon has also been observed in circular-cylinder flow control (Lu and Sato 1996). We shall return to this point as well as its relation with the shear-layer evolution in § 5. In addition to a high lift/drag ratio, in practice the amplitude of C_l and C_d should be as small as possible.

Thirdly, as $\widehat{f_e}$ reduced to 0.5, we have *subharmonic resonance with vortex shedding*. This leads to the largest lift increase (73.2 %) among all test cases, but the drag is also increased by 23.6% (the total normal force is increased by 41.8%). Many subharmonic modes are excited, but other modes are less suppressed compared to $\widehat{f_e} = 1$ and 2. On the

other hand, the largest drag reduction (5.5 %) occurs when $\hat{f}_e = 4$, but the lift increase is small. Therefore, the optimal lift enhancement, drag reduction, lift/drag-ratio increase, and amplitude alleviation, all occurred at different forcing frequencies. Note that some results (e.g., optimal forcing frequencies) are fairly close to experimental data (e.g., Zhou et al. 1993), though the airfoils are different.

4.2. Effect of Angle of Attack

At different angles of attack, similar pictures of C_l and C_d with various forcing frequencies were obtained. But, it is sufficient here to give the time-averaged values of lift, drag, and lift/drag ratio only. These are listed in Table 1, along with the relative amplitudes of lift and drag. Figures 10, 11, and 12 roughly outline the range of angle of attack for effective flow control: between 20° and 30°. The strongest effect occurs at $\alpha = 20°$, where the optimal enhancement of lift/drag ratio is as large as 57.7% at $\hat{f}_e = 1.0$. Interestingly, this is also the frequency with almost perfect lock-in phenomenon, similar to the case of $\alpha = 25°$ and $\hat{f}_e = 2.0$. For this angle of attack, additional computation was made with $\hat{f}_e = 1/3$ and 1.5; but no qualitative change was observed.

```
Figures 10 - 12 here
```

The effect of unsteady control quickly drops to the level of 10% both as α decreases only two degree below 20°, and as α increases beyond 30°. The physical reason for this will be discussed later.

Figure 13 adds the lift benefit due to forcing to the unforced curve, Fig. 1. The figure vividly indicates that the steep lift valley at static stall is largely fulfilled and further piled up till $\alpha = 35°$. Only a narrow lift valley near $\alpha_{stall} \simeq 12°$ (for $Re_c = 5 \times 10^5$) remains, which has a width of about 7 degrees. As noted before, this residual valley could be easily eliminated by sweeping the wing.

```
Figure 13 here
```

4.3. Time-Averaged Flow Field

Having obtained positive result on the lift enhancement by post-stall flow control, we now use the time-averaged flow-field behavior at $\alpha = 25°$ as an example to further understand the effect of forcing.

Figures 14 through 18 give the averaged streamlines, vorticity contours, and pressure distributions for different $\hat{f}_e$. Because the averaged flow field includes the nonlinear streaming effect (Wu at al. 1991), these patterns are not simply steady solutions of the

Navier-Stokes equation. Nevertheless, from the time-averaged field some basic features can be quickly identified.

```
┌─────────────────────────────────────────────────────────┐
│                   Figures 14 - 18 here                  │
└─────────────────────────────────────────────────────────┘
```

For the unforced case, there is a lifting vortex above the airfoil, which is however pushed up by its induced secondary separated vortex and a quite strong trailing vortex that invades deeply upstream. These three vortices of alternative signs, plus the leading-edge shear layer, are the basic constituents of the uncontrolled separated flow. The time-averaged pressure distribution on the upper surface is basically a flatform, $\overline{C}_p \simeq -1$, which confirms that the flow is indeed fully separated. Near the trailing edge there is a vortex-induced low pressure region.

When forcing is imposed, except for $\hat{f}_e = 4$ which has the same qualitative feature as unforced flow, the secondary separation is suppressed, and the mean trailing vortex is confined in a much smaller region behind the tailing edge. Note that the two or three leaves of the mean trailing-vorticity contours indicate that, before shedding off, the vortex wonders around the edge and stays longer at these positions in a period. This situation creates a much more comfortable circumstance for the main lifting vortex to be captured closer to the wing, and hence produce a larger lift. It should be noticed that the captured mean vortex is about as strong as that of the leading-edge vortex of a slender delta wing at the same angle of attack: it induces a $\overline{C}_p \simeq -2$ beneath the vortex.

A comparison of Figs. 16b and 17b further reveals some interesting difference between the two resonant states. When $\hat{f}_e = 2$, the mean shear layer has very smooth contours. It extends across the whole chord length, basically parallel to the free stream, and with an almost constant mean thickness. The mean trailing vortex is thereby pushed more downstream and confined in a even smaller region than that in Fig. 16b. Therefore, this nearly perfect resonant state at $\hat{f}_e = 2$ results in a narrower wake and smaller drag, as well as a much smaller amplitude of C_l and C_d as observed above. However, since at this forcing frequency the merging of leading-edge vortices into larger ones is blocked, the main lifting vortex is not as strong as that at $\hat{f}_e = 1.0$. This explains the observed reduction of lift enhancement at higher forcing frequencies.

Note that the mean-streamline patterns satisfy the topological rule for two-dimensional cross-sectional flow (Hunt et al. 1978):

$$\left(\sum_N + \frac{1}{2} \sum_{N'} \right) - \left(\sum_S + \frac{1}{2} \sum_{S'} \right) = -1,$$

where N, N', S, and S' stands for node, semi-node, saddle, semi-saddle, respectively. In Figs. 14a and 15a, we have $\sum_N = 3$, $\sum_{N'} = 0$, $\sum_S = 1$, and $\sum_{S'} = 6$; while in Figs. 16a,

17a, and 18a, these numbers are 1, 0, 0, 4, respectively. It is well known that the fewer the number of critical points is, the "healthier" would be the flow pattern — it would be more stable and easier to utilize. As conjectured by Wu and Wu (1992), the post-stall resonance between leading-edge shear layer and trailing-edge vortices, triggered off by a low-level forcing, precisely achieves such a goal.

4.4. Vorticity Field and Vortex Dynamics

In order to fully understand the specific fluid-dynamic mechanisms of post-stall flow control, we now display typical instantaneous vorticity contours at $\alpha = 25°$ and discuss their implications.

Figure 19 shows a few typical evolution stages of vortex dynamic evolution in a period for unforced flow. We see a strong, well rolled-up trailing vortex, secondary and tertiary separated vortices from the mid portion of upper surface, and a short leading-edge shear layer. Only the last one is favorable for lift, but after two to three small discrete vortices (the location of their formation is random for unforced shear layer), the favorable vortex is quite loose with low-level vorticity. Moreover, this weak vortex is raised up by the unfavorable vortices. As the strong trailing vortex stays above the rear part of the airfoil, the lift drops to the bottom; while as it sheds away, the lift climbs up. The zoom-out plot containing a few pair of shed vortices shows that the wake consists of a Kármán vortex street with an increasing width, in which the vortices of opposite signs are staggered.

```
Figure 19 here
```

The forced flow at $\hat{f}_e = 1.0$ is shown in Fig. 20. The leading-edge shear layer rolls into a strong coherent favorable vortex nearer to the airfoil. In a smaller part of the period the secondary vortex still has an effect, but weaker than unforced case. Meanwhile, the shrinking and moving downstream of the trailing vortex before it sheds off are obvious. The wake vortices are now aligned to almost a single array. Such a single vortex array behind an oscillating airfoil has been observed by, e.g., Cornish (1983) and Koochesfahani (1989), and in an acoustically excited circular-cylinder flow, by Detemple-Laake and Eckelmann (1989). Note that the uneven spacing between the wake vortices makes them in such a pair that a mutual induction creates an upwash. However, this does not imply a loss of lift: for unsteady flow the force cannot be solely judged by the flow behavior over a control surface in the wake. In the mean vorticity contours (Fig. 16a) the upwash disappears.

```
Figure 20 here
```

Recalling the results of § 3, we may interpret the main vortex-dynamics mechanisms that cause the difference between forced and unforced flow patterns as follows.

First, the forcing with a low frequency such as

$$f_e = f^0_{\text{shed}} = 0.152 f^0_{\text{shear}}$$

causes several small discrete vortices, formed from high-frequency shear-layer instability, to quickly merge into a large vortex. In addition, in § 3.1.2 we mentioned that a forcing with $c_\mu = 1\%$ did not enhance the lift, i.e., the forcing strength must be above a certain level. Therefore, we identify the vortex merging as a typical *rolling-up coalescence* addressed in § 2.2. From computed vorticity contours, a merging of three vortices can be recognized. We mention that, compared to $\hat{f}_e = 1.0$, when $\hat{f}_e$ reduces to 0.5 the rolling-up coalescence involves more vortices and produces a larger vortex with higher strength (not shown); thus the maximal lift enhancement occurs at the low frequency end.

Second, since the main vortex has a rolling-in structure, when it is strong enough it will have the ability of *entraining* most disordered fluid into its core. This seems to be the fluid-dynamic mechanism of frequency lock-in for this special flow. Note that for two-dimensional *steady* flow the rolling-in is impossible.

Third, the entrainment of strong lifting vortex is asymmetric on its upper and lower sides. Due to the existence of airfoil surface, on its lower side not much fluid is entrained. The main entrainment occurs on its upper side, where the fresh stream brings larger momentum into the vortex, so the vortex has a tendency of turning downward. This is a very favorable effect. Since most of disorganized secondary and tertiary separated flow disappear, once saturated, the main vortex tends to be advected along the main stream direction, closer to the airfoil surface than unforced case. Therefore, the upstream invading of trailing vortices due to the induction as the main vortex travel above it, as in the unforced case, is also greatly suppressed. The circulation around the airfoil is thus more favorable.

With the above explanation, the flow patterns under other flow and forcing parameters can also be better understood. For example, as $\hat{f}_e$ increased to 2.0 (Fig. 21), the size and strength of both lifting vortex and trailing vortices are reduced. It seems that the forcing at this f_e can take very good care of both high-frequency shear layer and low-frequency shedding. Two lifting vortices with nice circular shape now coexist above the wing, and the unfavorable interference of the trailing vortex is further limited. The wake vortices also remarkably align to a single array with even spacing (hence no upwash). The doubling of forcing frequency implies that the rolling-up coalescence occurs at a smaller scale than before, and so is the trailing vortex formation. Therefore, the wake width is narrower. This further explains why the amplitude of C_l and C_d is greatly reduced.

Figure 21 here

The favorable effect of forcing declines as $\hat{f}_e$ further increases to 4.0 (Fig. 22), where we have $f_e/f^0_{\text{shear}} = 0.606$, which is of order one. Thus, as explained by Ho and Nosseir

(1981), the shear layer is simply discretized to a series of traveling vortices but no rolling-up coalescence happens. Note that, in contrast to the case of $\hat{f_e} = 2.0$, while the number of leading-edge vortices is doubled and their strength is halved, now the trailing vortex is *not*. Meanwhile, the small traveling vortices are not strong enough to entrain most of disorganized fluid. Consequently, the response shedding frequency no longer follows f_e, and the irregular secondary and tertiary separation reoccur. As a result, the drag is still reducing but the lift enhancement is small.

<div style="border:1px solid black; text-align:center; padding:1em;">Figure 22 here</div>

We stress that the first and second mechanisms, i.e., the rolling-up coalescence and strong entrainment, are both necessary. Even if the coalescence appears, the vortex formed thereby may be too far from the airfoil surface so that it cannot entrain most disorganized fluid. In this case the flow field will still behave like an unforced flow. This indeed happens at $\alpha = 30°$ (not shown). The strong remaining disorganized flow will reversely make the coalescence process aperiodic. This is the main reason for the observed much smaller lift enhancement.

4.5. Necessary Conditions for Post-Stall Lift Enhancement

Based on the above results, we may summarize the physical mechanisms of lift enhancement at post-stall angles of attack by unsteady control as follows: a proper forcing locks the instability frequencies of leading-edge shear layer and trailing vortices at a frequency equal to the harmonics and subharmonics of the forcing frequency. The result of resonance includes: the suppression of secondary and tertiary separations; the modulation of shear-layer evolution, entrainment, and its moving downward; and the shrinking and downstream shifting of trailing vortices. Consequently, a lifting vortex is captured in time-average sense, and the uncontrolled random separated flow becomes well organized. The three elements, i.e., the leading-edge shear layer, trailing vortices, and the airfoil, form a resonance cavity under a low-level forcing.

Based on this understanding, therefore, the following two basic conditions for post-stall lift enhancement are necessary:

(1) The co-existence of a well-developed free shear layer and trailing vortices.

(2) A well shaped "resonant cavity" enclosed by leading shear layer, trailing vortices, and upper surface of the wing.

In the first condition, the shear layer must be *free* enough to undergo the local instability, discretization, pairing, and rolling-up coalescence. Only in this case can these processes be effectively modulated by forcing. For α too close to α_{stall}, the shear layer is

too close to the surface (as observed at $\alpha = 18°$; the figure is not shown) and loses part of its freedom of being modulated. Thus, the forcing effect reduces.

In the second condition, the "resonant cavity", now bounded by deformable fluid and has different boundary conditions as a solid-bounded cavity, cannot be too large. For otherwise the intrinsic communication between the shear layer and trailing vortices will be too weak. This happens for $\alpha \geq 35°$, and explains why the forcing effect is declined at a too large angle of attack. Moreover, this condition also emphasizes the importance of the airfoil shape.

5. Concluding Remarks

The present study provides an unambiguous numerical evidence to the post-stall lift enhancement. Along with existing experimental results, it can be asserted with confidence that the effect does exist and could be very beneficial.

The physics behind the post-stall lift enhancement proposed by Wu et al. (1991) is further identified. The shear-layer instability and receptivity are the key to an effective unsteady control, and the resonance between leading and trailing vortices with frequency locked into the harmonics of forcing frequency is the main mechanism that leads to a favorable flow pattern. In average, the secondary separation is suppressed, and the trailing vortex is confined to downstream of the airfoil. Therefore, the lift is increased (never decreased as noticed in experiments). If the forcing is at a harmonic of shedding frequency, the drag, as well as the amplitudes of oscillating lift and drag, can be reduced.

As mentioned in the Introduction, the post-stall lift enhancement by unsteady control, as numerically confirmed and physically understood by our two-dimensional study, can be further improved by sweeping the wing. Then a monotonic increase of lift is possible for the whole range of $0° \leq \alpha \leq \alpha_m$, such that one can enjoy a new freedom to use the vortical lift on a wing at a very high angle of attack, with the flow being completely separated. The post-stall control greatly enhances such a vortical lift, i.e., more favorable deviation from (2a). From the practical point of view, in order to reach this goal, more works need to be down in the future. For example, more complex turbulence models could be used to include the spanwise perturbation and correlation while the basic flow is still two-dimensional; the Reynolds number could be increased in both experimental and numerical studies; the sweeping effect and the fully three-dimensional configuration should be examined; and finally, the optimal wing configuration as well as other factors affecting the control (as stated in § 2.3) should be investigated. Some of these works are being undertaken.

It must be stressed again that our numerical results are merely preliminary. Except for the necessity of extending the computation to more realistic three-dimensional configurations and higher Reynolds numbers, as a two-dimensional computation, the results still suffer from some shortages.

First, The entire flow field was assumed turbulent, which was then accounted for by a simple two-dimensional algebraic model. Thus, the important effect of transition to turbulence and three-dimensional turbulence were far from fully explored.

Second, the Reynolds-number effect was not systematically studied. This brings some further uncertain factors in judging the value of our results, due to the possible existence of a critical regime. While we have no idea on when this regime will appear for the post-stall airfoil flow, some preliminary signs indicate that it may be quite close to $Re_c = 5 \times 10^5$. Except the example given by Rumsey et al. (1987), our own insufficient tests with an one-equation turbulence model also showed a steady asymptotic behavior of lift and drag is possible in some nearby Reynolds numbers and angles of attack. Note that so far no turbulence model has been developed and fully tested specifically for unsteady separated flows including transition. In our case, it would not be surprising if different existing models predict different lower and upper bounds of Reynolds number for the critical regime.

Obviously, these two problems are closely related. They should be fully addressed in our future work. However, the critical regime without vortex shedding is nevertheless a special situation compared to the much wider range of practical Reynolds numbers ($10^6 \sim 10^8$), and in most cases the unsteady shedding and control are much more generic.

To conclude this report, we briefly consider the specific circumstances where the post-stall flow control technique is very useful.

As said before, from the viewpoint of aerodynamic efficiency (the cruise condition), the optimal use of vortical lift is in the regime of attached flow. Any flow control cannot change this basic fact. However, the *steady detached-vortex flow* has been widely used on slender wings or leading-edge extensions, mainly for maneuvering. This is the second generation of flow type in aeronautics, and has greatly enlarged the range of usable angles of attack for proper configurations. Now we are facing the third generation of flow type, which is unsteady and could be used at an even larger range of angles of attack, as long as the low drag is not a key issue to address. In practice, this happens at least in the following cases:

(1) Landing of aircraft with flap deployed;

(2) Highly maneuvering flight.

In the first case, the technique can be applied to a flap. The increased drag on flap at post-stall angle of attack is only a small portion of the aircraft drag, which is beneficial in landing. The use of post-stall control would reduce the flap size and weight by enlarging its usable angle of attack. In the second case, the drag increase is not a problem (even a favorable effect) and the technique could be used on the main wing: we believe that the technique of post-stall lift enhancement by unsteady control can well be applied not only large-aspect-ratio wings, but also slender wings.

References

Baldwin, B.S. and Lomax, H. 1978. Thin layer approximation and algebraic model for separated turbulent flows. *AIAA 78-257*.

Batchelor, G.K. 1956. Unsteady laminar flow with closed streamlines at large Reynolds number. *J. Fluid Mech.* **1**, 177-190.

Betz, A. 1950. Wie entsteht ein Wirbel in einer wenig zähen Flüssigkeit? *Naturwissen.* **37**, 193-196.

Chang, R.C., Hsiao, F.-B., and Shyu, R.-N. 1992. Forcing level effects of internal acoustic excitation on the improvement of airfoil performance. *J. Aircraft* **29**, 823-829.

Chernyshenko, S.I. 1995. Stabilization of trapped vortices by alternating blowing-suction. *Phys. Fluids* **7**, 802-807.

Collins, F.G. and Zelenevitz, J. 1975. Influence of sound upon separated flow over wings. *AIAA J.* **13**, 408-410.

Critzos, C.C., Heyson, H.H., and Boswinkle, R.W. 1955. Aerodynamic characteristics of NACA 0012 airfoil section at angles of attack from 0° to 360°. *NACA TN 3361*.

Fage, A. and Johasen, F.C. 1927. On the flow of air behind an inclined flat plate of infinite span. *Proc. Roy. Soc. Lond.* **A116**, 170-197.

Güven, O., Farell, C., and Patel, V.C. 1980. Surface-roughness effects on the mean flow past circular cylinders. *J. Fluid Mech.* **98**, 673-701.

Ho, C.-M. and Huang, L.-S. 1982. Subharmonics and vortex merging in mixing layers. *J. Fluid Mech.* **119**, 443-473.

Ho, C.-M. and Huerre, P. 1984. Perturbed free shear layers. *Ann. Rev. Fluid Mech.* **16**, 365-424.

Ho, C.-M. and Nosseir, N.S. 1981. Dynamics of an impinging jet. Part I. The feedback phenomenon. *J. Fluid Mech.* **105**, 119-142.

Hsiao, F.-B., Liu, C.-F., and Shyu, J.-Y. 1990. Control of wall-separated flow by internal acoustic excitation. *AIAA J.* **28**, 1440-1446.

Hsiao, F.-B., Wang, T.-Z., and Zohar, Y. 1993. Flow separation control of a 2-D airfoil by a leading-edge oscillating flap. *Intern. Conf. Aerospace Sci. Tech.*, Dec. 6-9, 1993, Tainan, Taiwan.

Hsiao, F.-B., Shyu, R.-N., and Chang, R.C. 1994. High angle-of-attack airfoil performance improvement by internal acoustic excitation. *AIAA J.* **32**, 655-657.

Huerre, P. and Monkewitz, P.A. 1990. Local and global instabilities in spatially developing flows. *Ann. Rev. Fluid Mech.* **22**, 473-537.

Hunt, J.C.R., Abell, C.J., Peterla, J.A., and Woo, H. 1978. Kinematical studies of the flows around free or surface mounted obstacles: applying topology to flow visualization. *J. Fluid Mech.* **86**, 179-200.

Jones, G.W. Jr., Cincotta, J.J., and Walker, W.W. 1969. Aerodynamic forces on a stationary and oscillating circular cylinder at high Reynolds numbers. *NASA TR R-300.*

Ko, S. and McCroskey, W.J. 1995. Computations of unsteady separating flows over an oscillating airfoil. *AIAA 95-0312.*

Lamb, H. 1932. *Hydrodynamics.* Cambridge University Press.

Launder, B.E. and Sharma, B.I. 1974. Application of the energy-dissipation model of turbulence to the calculation of flow near a spinning disc. *Lett. Heat Mass Transfer* **1**, 131-138.

Oertel, H. Jr. 1990. Wake behind bunt bodies. *Annu. Rev. Fluid Mech.* **22**, 539-564.

Patel, V.P., Rodi, W. and Scheuerer, G. 1985. Turbulence models for near-wall and low Reynolds number flows: A review. *AIAA J.* **23**, 1308-1319.

Rockwell, D.O. 1972. External excitation of plan jets. *Trans. ASME* E: *J. Appl. Mech.* **39**, 883-890.

Rockwell, D. 1990. Active control of globally-unstable separated flows. *Intern. Symp. Nonsteady Fluid Dynamics*, June 4-7, 1990, Ontario, Canada. J.A. Miller and D.P. Telionis eds., ASME, pp. 379-394.

Roshko, A. 1954a. A new hodograph for free-streamline theory. *NACA TN 3168.*

Roshko, A. 1954b. On the drag and shedding frequency of two-dimensional bluff bodies. *NACA TN 3169.*

Roshko, A. 1961. Experiments on the flow past a circular cylinder at very high Reynolds number. *J. Fluid Mech.* **10**, 345-356.

Seifert, A., Bachar, T., Koss, D., Shepshelovich, M., and Wygnanski, I. 1993. Oscillatory blowing: a tool to delay boundary-layer separation. *AIAA J.* **31**, 2052-2060.

Spalart, P.R. and Allmaras, S.R. 1992. A one-equation turbulence model for aerodynamic flows. *AIAA 92-0439.*

Stansby, P.K. 1976. The lock-on of vortex shedding due to the cross-stream vibration of circular cylinders in uniform and shear flows. *J.Fluid Mech.* **74**, 641-665.

Thompson, K.W. 1990. Time-dependent boundary conditions for hyperbolic systems, II. *J. Comput. Phys.* **89**, 439-461.

Unal, M.F. and Rockwell, D. 1988. On vortex formation from a cylinder. Part I. The initial instability. *J. Fluid Mech.* **190**, 491-512.

Wick, B.H. 1954. Study of the subsonic forces and moments on an inclined plate of infinite span. *NACA TN 3221.*

Williamson, C.H.K. 1996. Vortex dynamics in the cylinder wake. *Annu. Rev. Fluid Mech.* **28**, 477-539.

Wu, J.M. and Wu, J.Z. 1992. Vortex lift at a very high angle of attack with massively separated unsteady flow. *IUTAM Symp. Fluid Dynamics of High Angle of Attack*, Sept. 13-17, 1992, Tokyo, Japan. Also: R. Kawamura and Aihara (eds.), *Fluid Dynamics of High Angle of Attack*, 1993, Springer-Verlag, 35-63.

Wu, J.Z. and Wu, J.M. 1996. Vorticity dynamics on boundaries. *Adv. Appl. Mech.* **32**, J.W. Hutchinson and T.Y. Wu (eds.), Academic Press, 119-275.

Wu, J.Z., Vakili, A.D., and Wu, J.M. 1991. Review of the physics of enhancing vortex lift by unsteady excitation. *Prog. Aerospace Sci. 28*, ed. by A.D. Young, Pergamon Press, 73-131.

Zhou, M.D., Fernholz, H.H., Ma, H.Y., Wu, J.Z., and Wu, J.M. 1993. Vortex capture by a two-dimensional airfoil with a small oscillating leading-edge flap. *AIAA 93-3266.*

Table 1

Time-Averaged Effect of Forcing at Different Frequencies and Angles of Attack

Cl – averaged lift coefficient
Cd – averaged drag coefficient
Cl_{rms} – r.m.s. value of lift coefficient
Cd_{rms} – r.m.s. value of drag coefficient

(a) $\alpha = 18°$

$\hat{f_e}$	Cl	Cd	L/D	Benefit $L/D\%$	Cl_{rms}	Cd_{rms}
0.0	0.988	0.261	3.785		0.073	0.017
0.5	0.952	0.227	4.194	10.81	0.149	0.042
1.0	0.891	0.223	4.005	5.81	0.125	0.059
2.0	0.987	0.233	4.236	11.92	0.084	0.035
4.0	1.003	0.238	4.214	11.33	0.085	0.026
8.0	0.989	0.242	4.087	7.97	0.091	0.028

(b) $\alpha = 20°$

$\hat{f_e}$	Cl	Cd	L/D	Benefit $L/D\%$	Cl_{rms}	Cd_{rms}
0.0	0.968	0.388	2.495		0.194	0.052
1/3	1.370	0.419	3.269	31.0	0.312	0.171
0.5	1.395	0.397	3.514	40.8	0.294	0.149
1.0	1.275	0.324	3.935	57.7	0.134	0.077
1.5	1.042	0.296	3.520	41.1	0.120	0.075
2.0	1.003	0.306	3.278	31.4	0.130	0.057
4.0	1.066	0.338	3.154	26.4	0.116	0.048

(c) $\alpha = 25°$

$\widehat{f_\epsilon}$	Cl	Cd	L/D	Benefit $L/D\%$	Cl_{rms}	Cd_{rms}
0.0	1.017	0.543	1.873		0.295	0.138
0.5	1.761	0.671	2.624	40.1	0.256	0.248
1.0	1.540	0.551	2.795	49.2	0.302	0.230
2.0	1.382	0.503	2.748	46.7	0.120	0.094
4.0	1.187	0.488	2.432	29.8	0.150	0.084

(d) $\alpha = 30°$

$\widehat{f_\epsilon}$	Cl	Cd	L/D	Benefit $L/D\%$	Cl_{rms}	Cd_{rms}
0.0	1.125	0.729	1.543		0.299	0.162
0.5	1.740	0.935	1.861	20.6	0.388	0.278
1.0	1.714	0.919	1.865	20.9	0.427	0.299
2.0	1.615	0.844	1.914	24.0	0.259	0.175

(e) $\alpha = 35°$

$\widehat{f_\epsilon}$	Cl	Cd	L/D	Benefit $L/D\%$	Cl_{rms}	Cd_{rms}
0.0	1.267	0.985	1.286		0.308	0.194
0.5	1.457	1.083	1.345	4.59	0.412	0.277
1.0	1.596	1.143	1.396	8.55	0.428	0.287
2.0	1.696	1.226	1.383	7.54	0.372	0.226
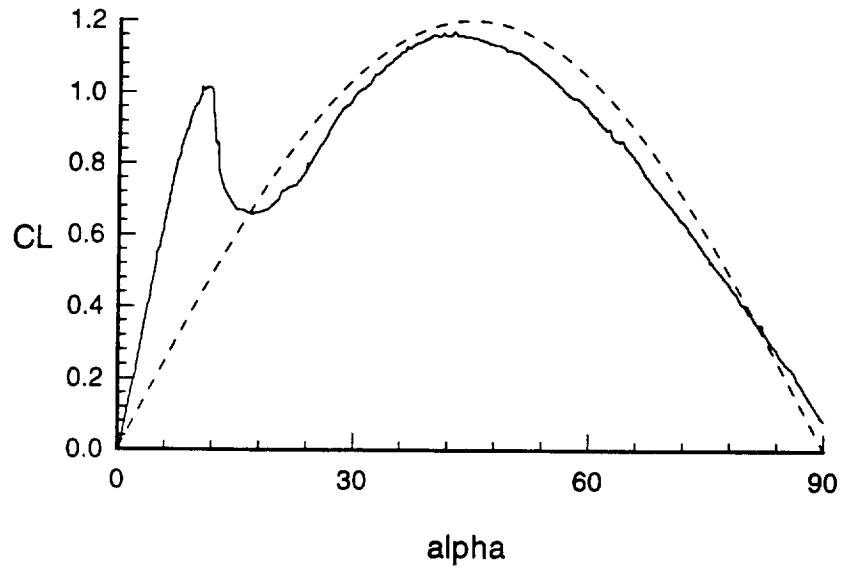
Figure 1. Lift coefficient C_l of NACA-0012 airfoil. From the experiments of Critzos et al. (1955), $Re = 5 \times 10^5$. Also shown (dash line) is a simple estimate for the post-stall C_l by Eq. (2a).
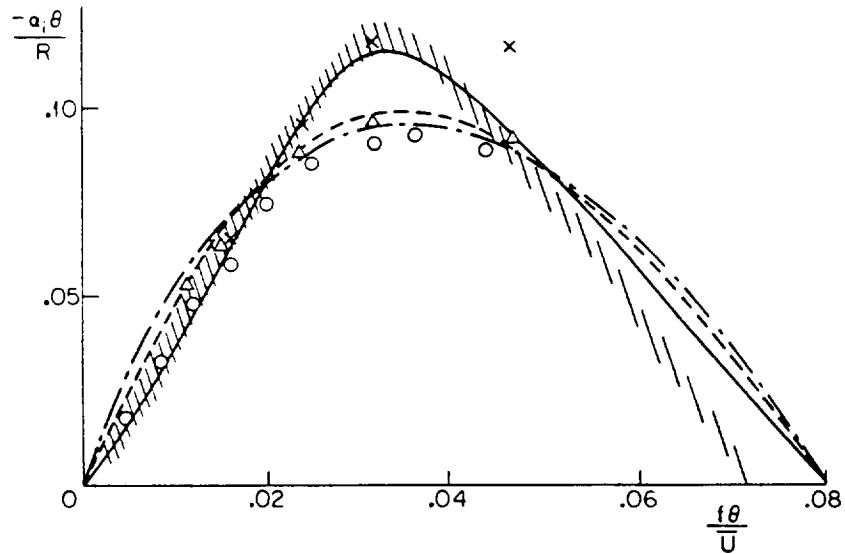
Figure 2. Variation of normalized amplification rate of perturbed shear layers with Strouhal number $f\theta/\overline{U}$. From Ho and Huerre (1984). Lines are results of linear stability theory and symbols from experiments, for different values of $R = (U_1 - U_2)/(2\overline{U})$.
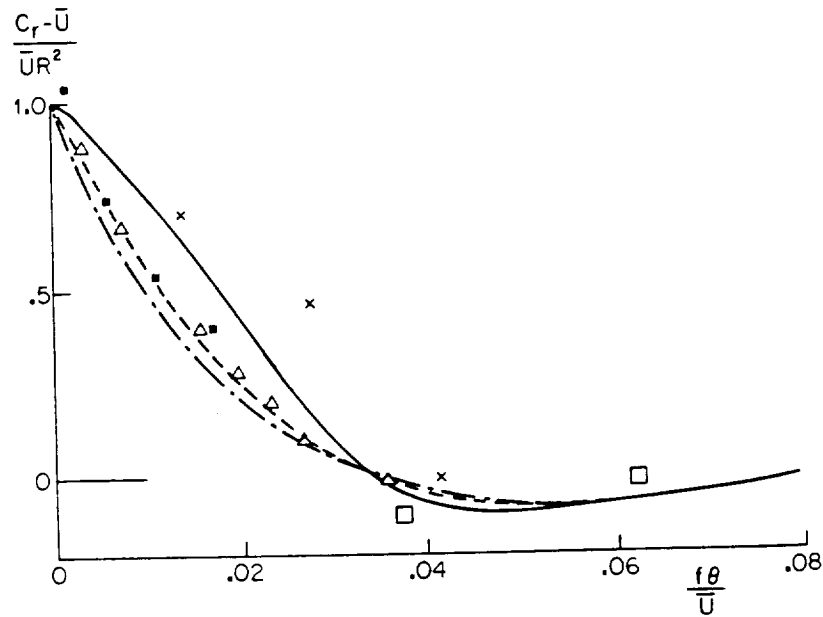
Figure 3. Variation of normalized phase velocity of perturbed shear layers with St. From Ho and Huerre (1984). Lines are results of linear stability theory and symbols from experiments, for different values of $R = (U_1 - U_2)/(2\overline{U})$.
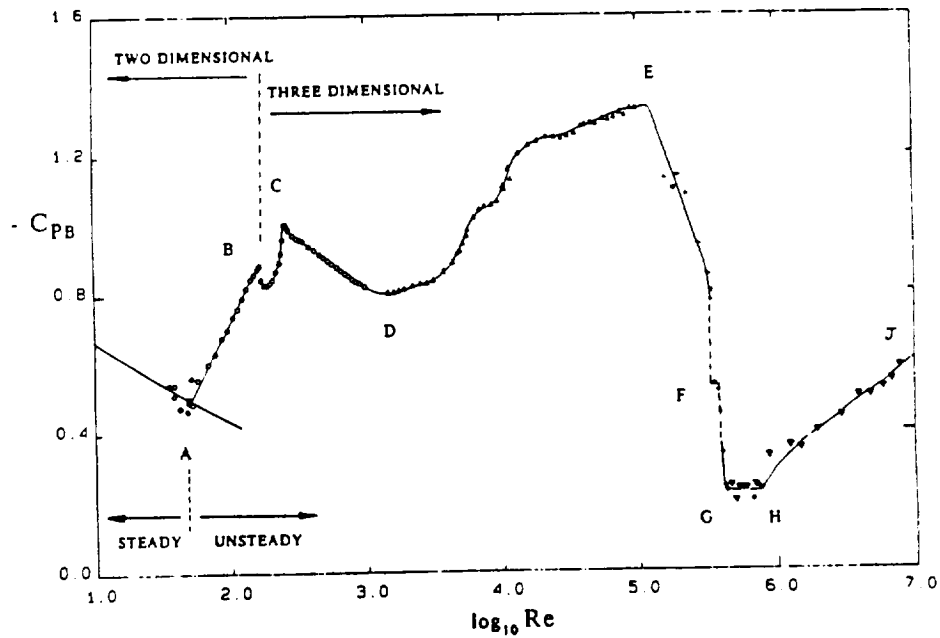
Figure 4. Base suction coefficients of cylinder over a large range of Reynolds numbers. From Williamson (1996).
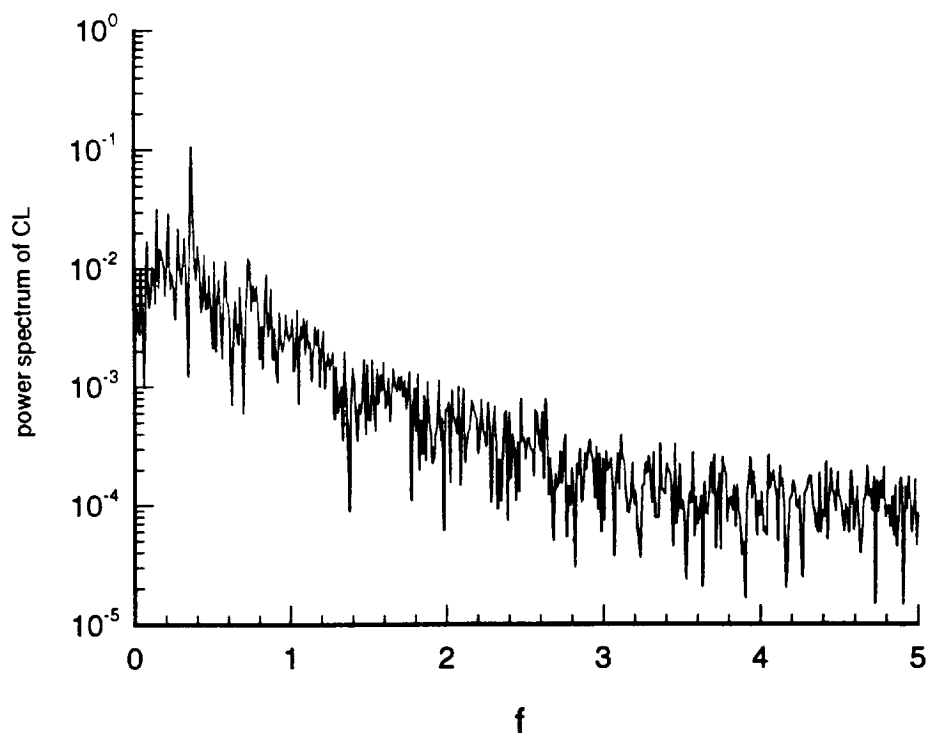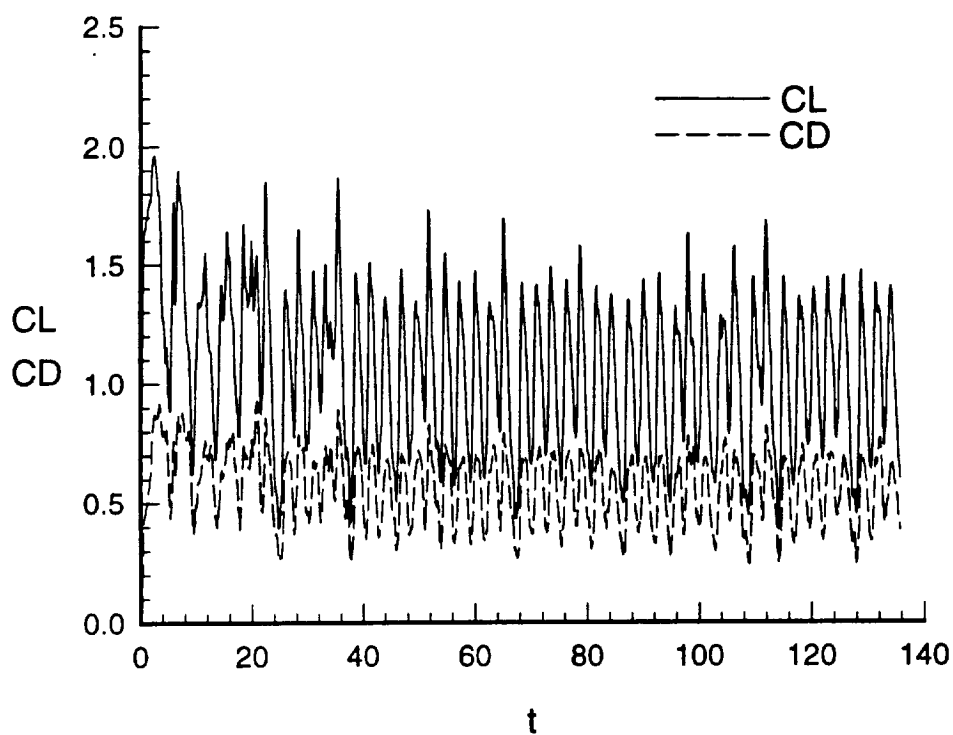
Figure 5. Computed unsteady force character of NACA-0012 airfoil. Uncontrolled flow. $Re = 5 \times 10^5$, $M = 0.2$, $\alpha = 25°$. The dimensionless time t and frequency f in this and following figures are scaled by U_∞ and chord-length c. (a) instantaneous lift and drag coefficients. (b) Power spectral density of C_l.
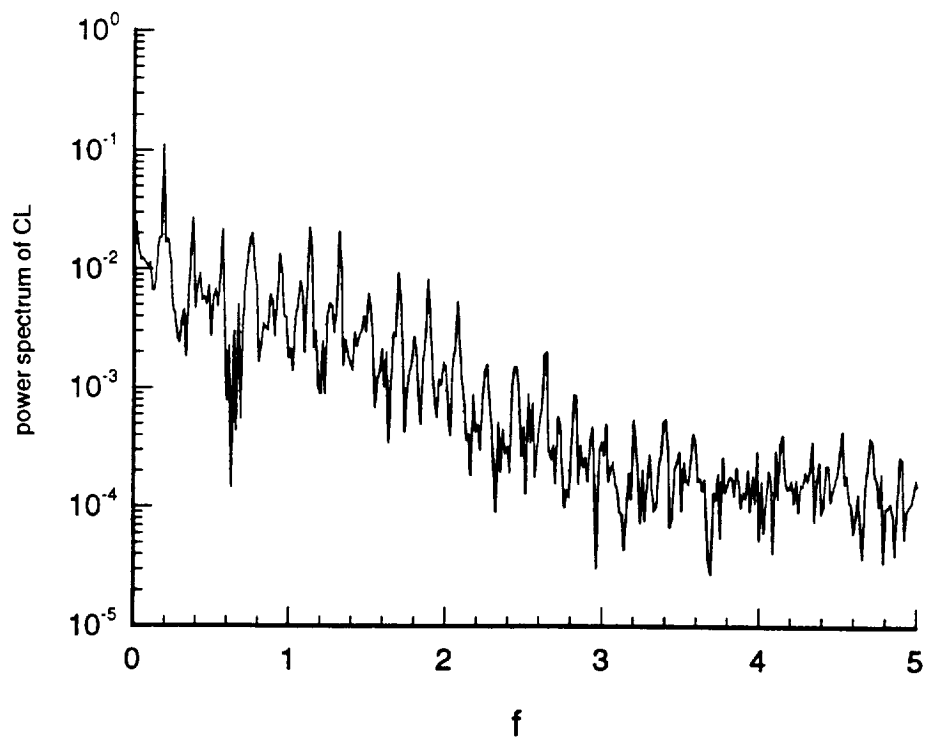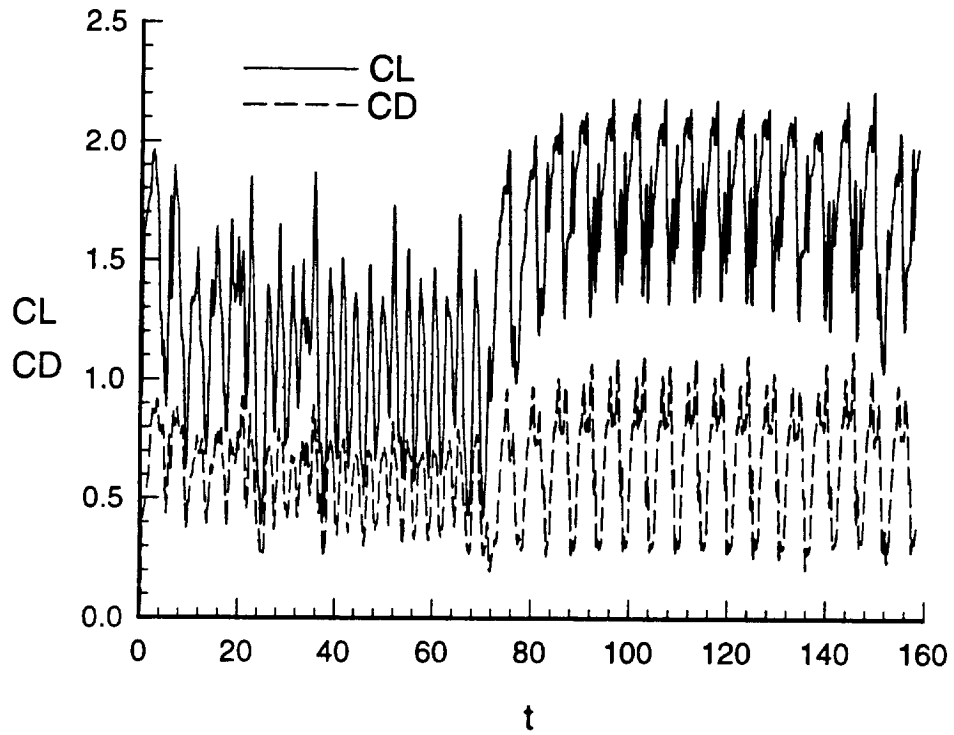
Figure 6. Unsteady force character of NACA-0012 airfoil. $\widehat{f_e} = 0.5$, $c_\mu = 2.5\%$. (a) instantaneous lift and drag coefficients. (b) Power spectral density of C_l. Flow condition is the same as Fig. 5.
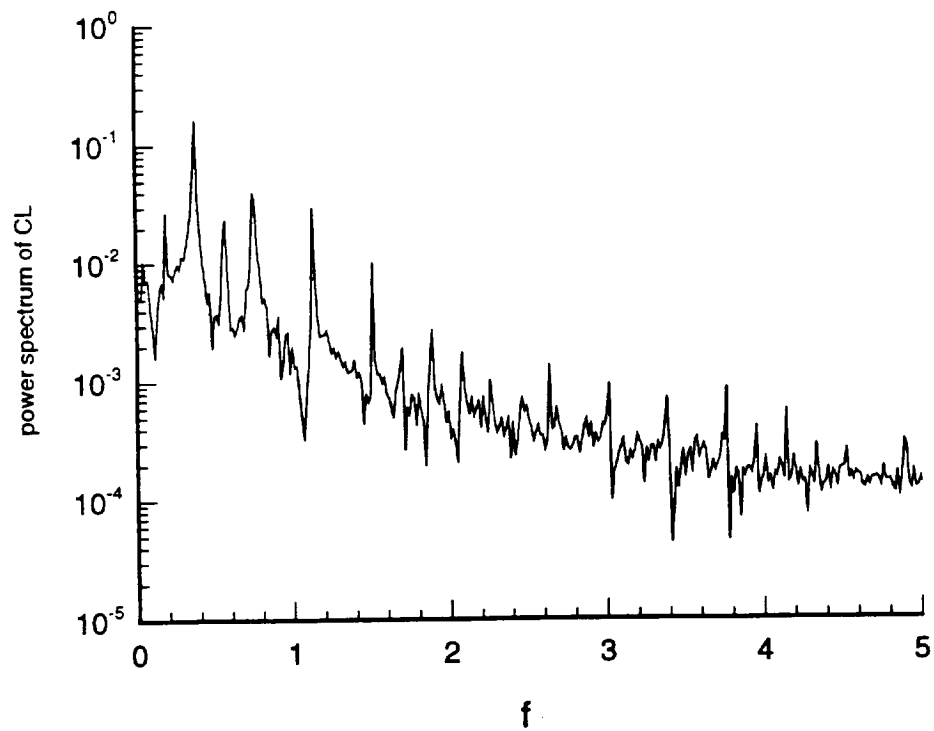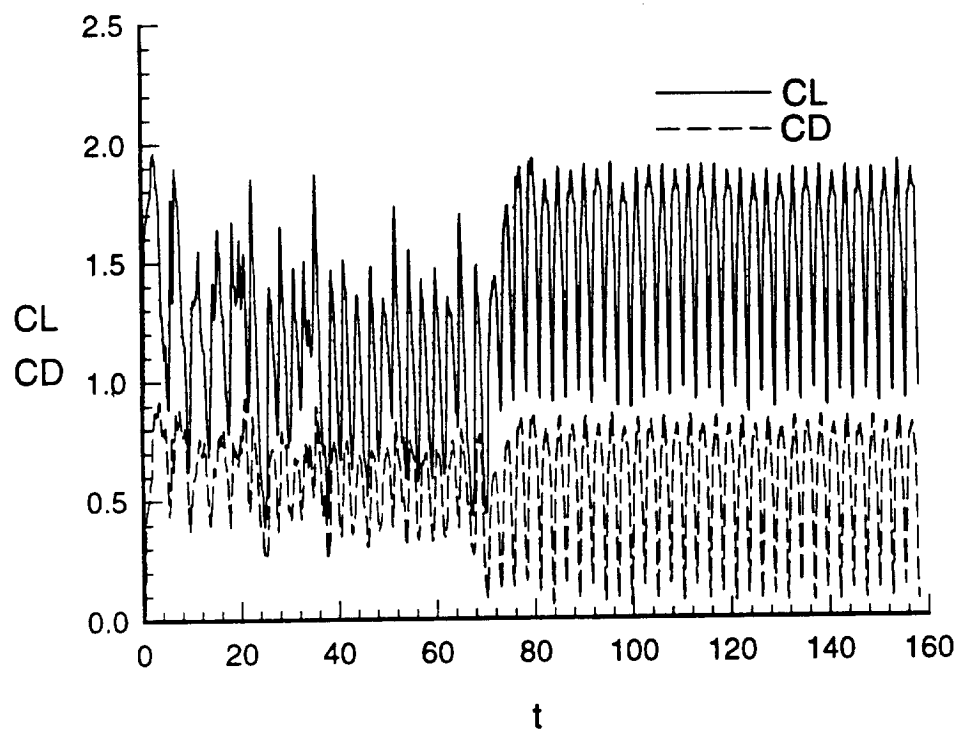
Figure 7. The same as Fig. 6; but $\widehat{f_e} = 1.0$.
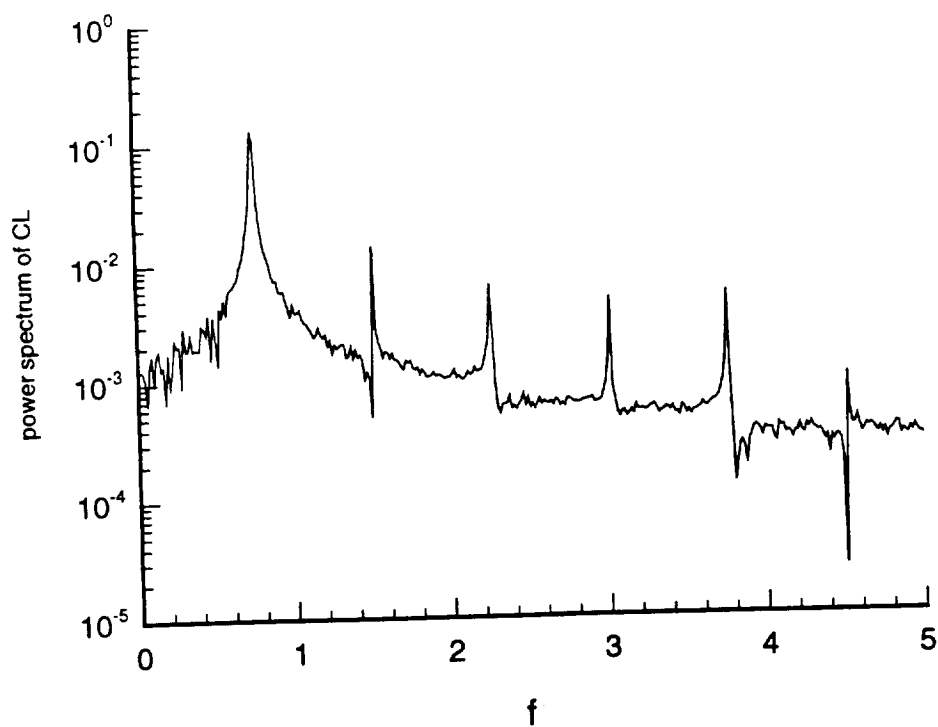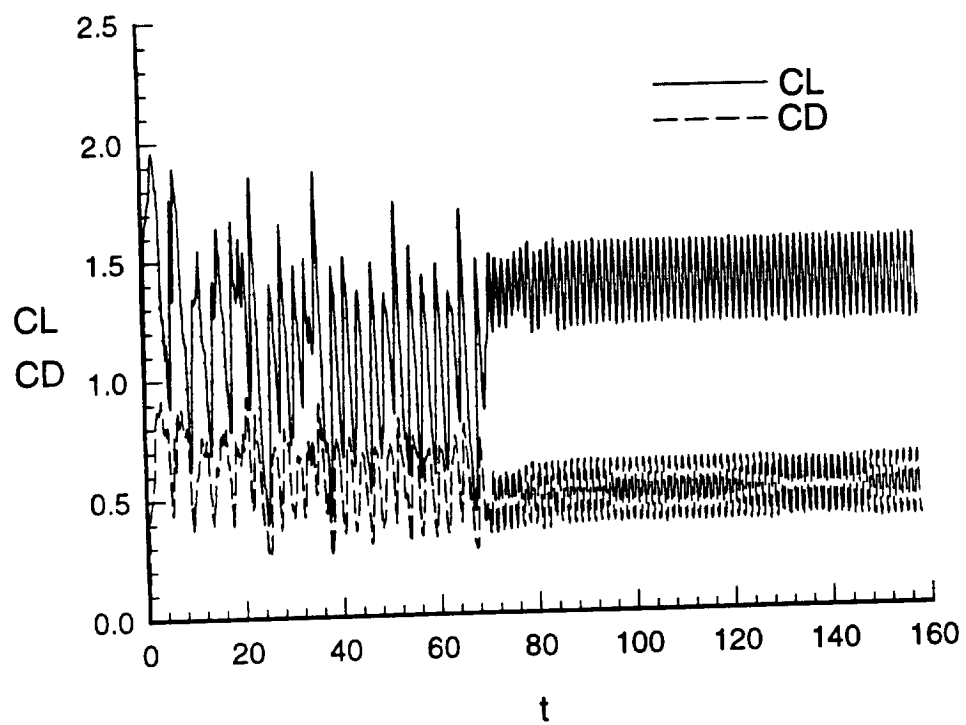
Figure 8. The same as Fig. 6; but $\widehat{f}_e = 2.0$.
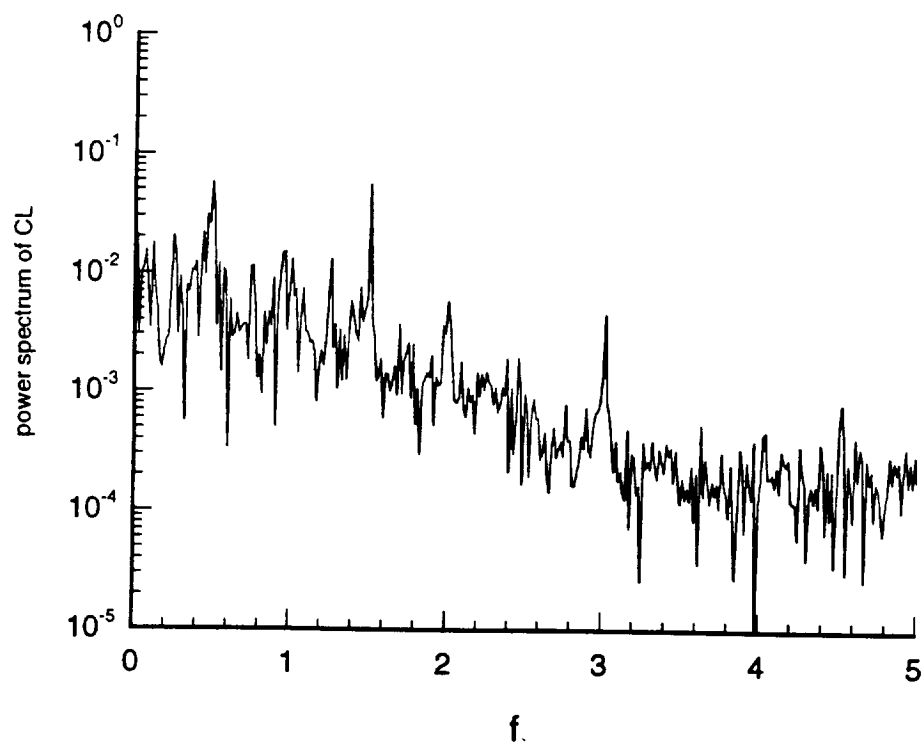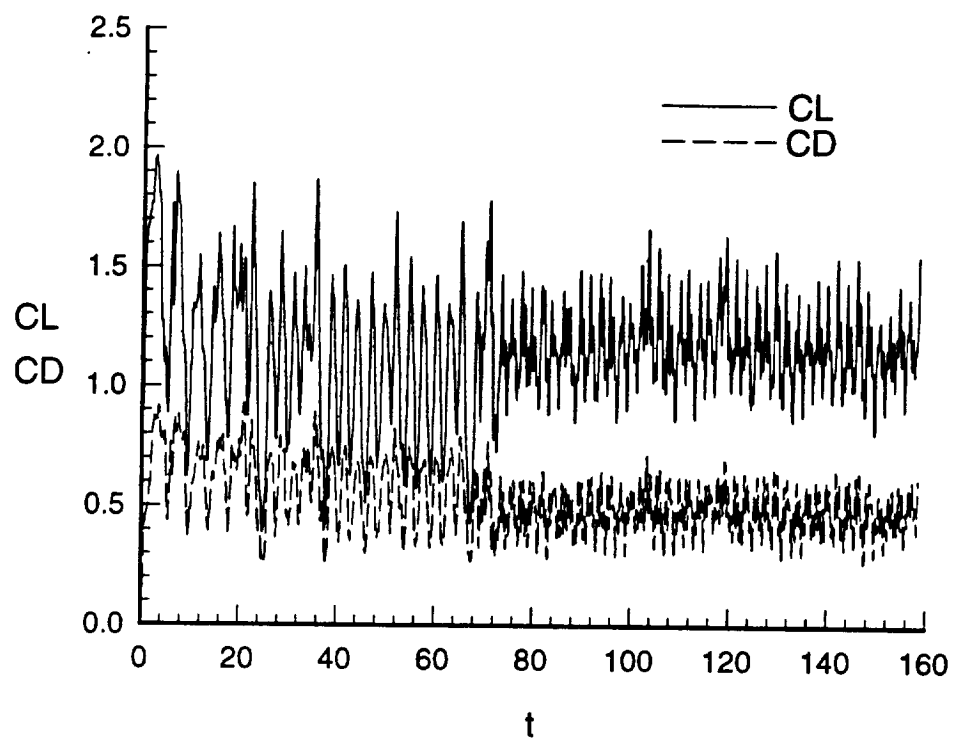
Figure 9. The same as Fig. 6; but $\widehat{f_e} = 4.0$.
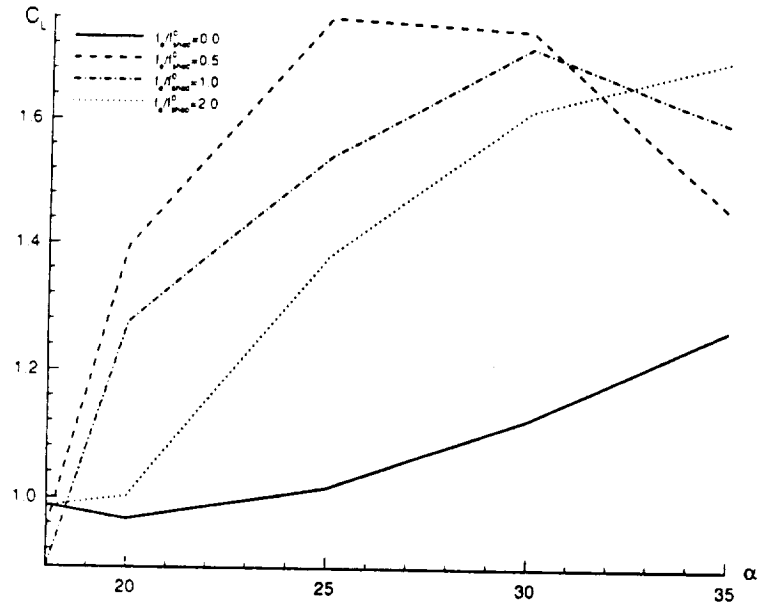
Figure 10. Controlled and uncontrolled averaged lift coefficients of NACA-0012 airfoil at different post-stall angles of attack.
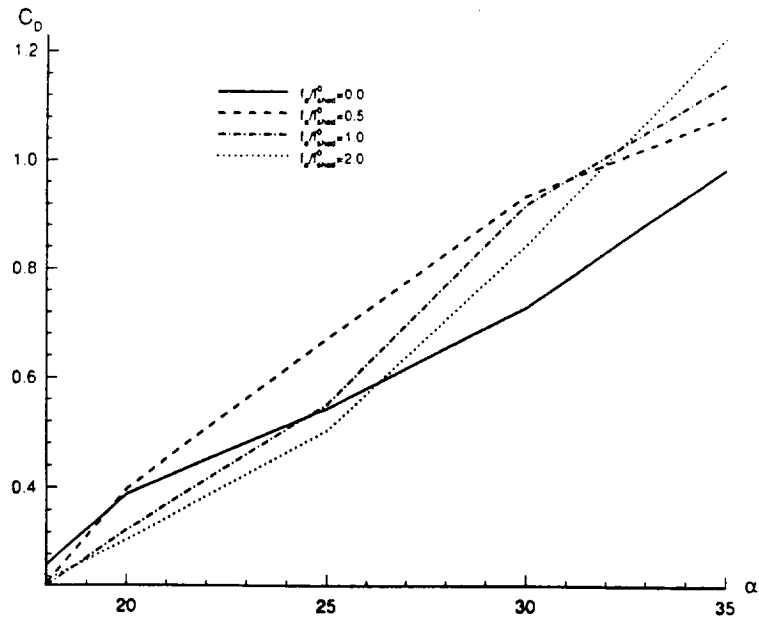
Figure 11. Controlled and uncontrolled averaged drag coefficients of NACA-0012 airfoil at different post-stall angles of attack.
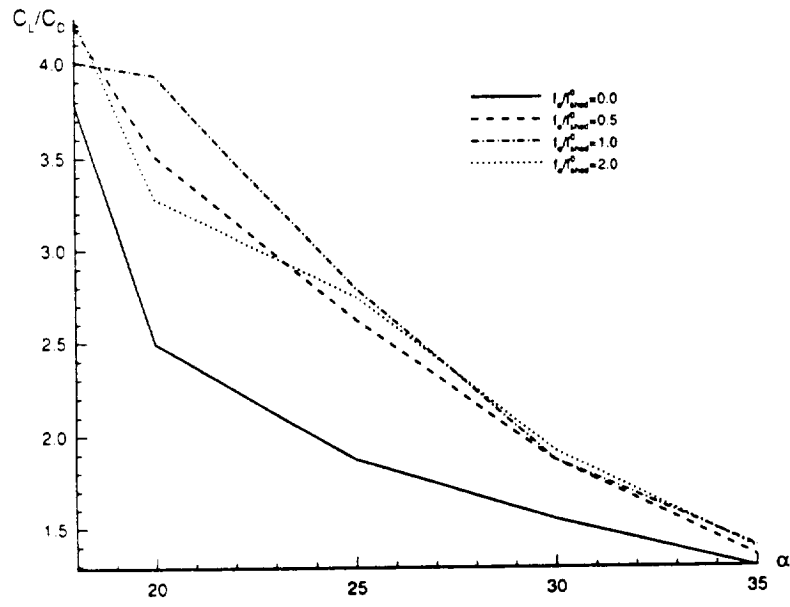
Figure 12. Controlled and uncontrolled averaged lift/drag ratio of NACA-0012 airfoil at different post-stall angles of attack.
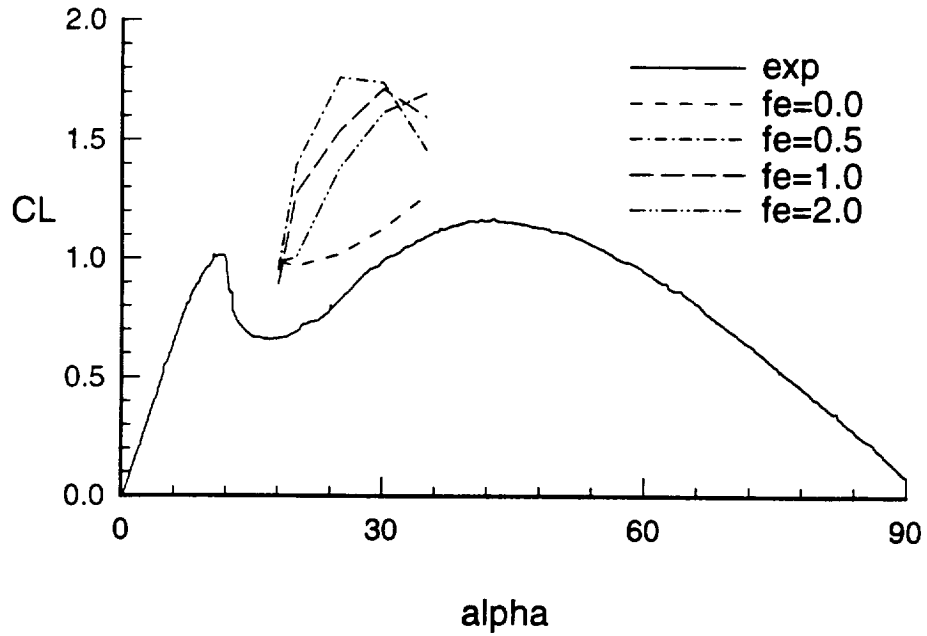
Figure 13. Overall view of the mean lift coefficient increase due to forcing.
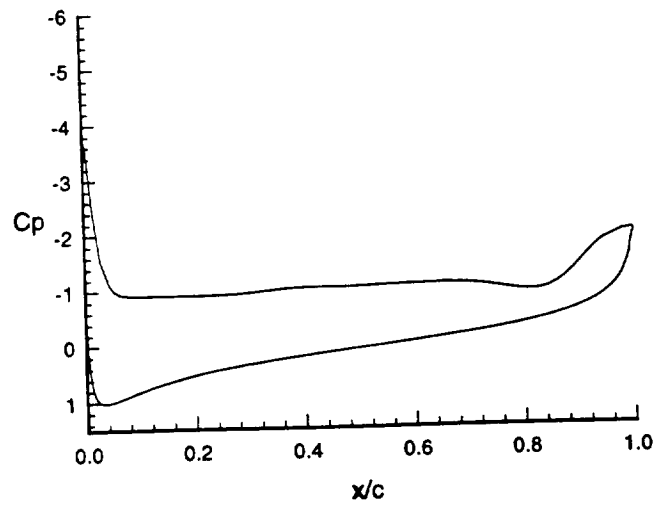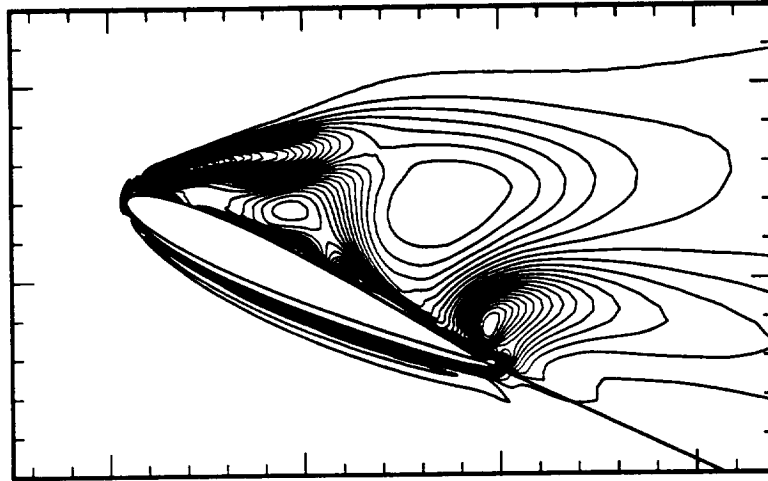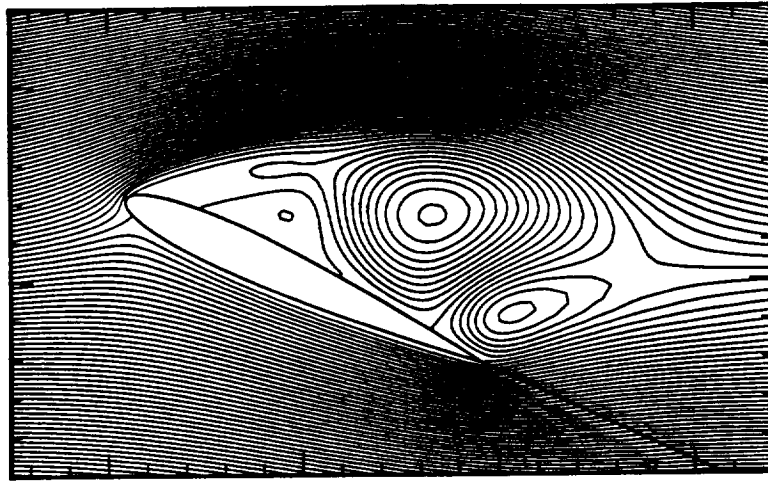
Figure 14. Time-averaged Streamlines (a), vorticity contours (b), and pressure coefficient (c) of NACA-0012 airfoil. The flow conditions are the same as that of Fig. 5.
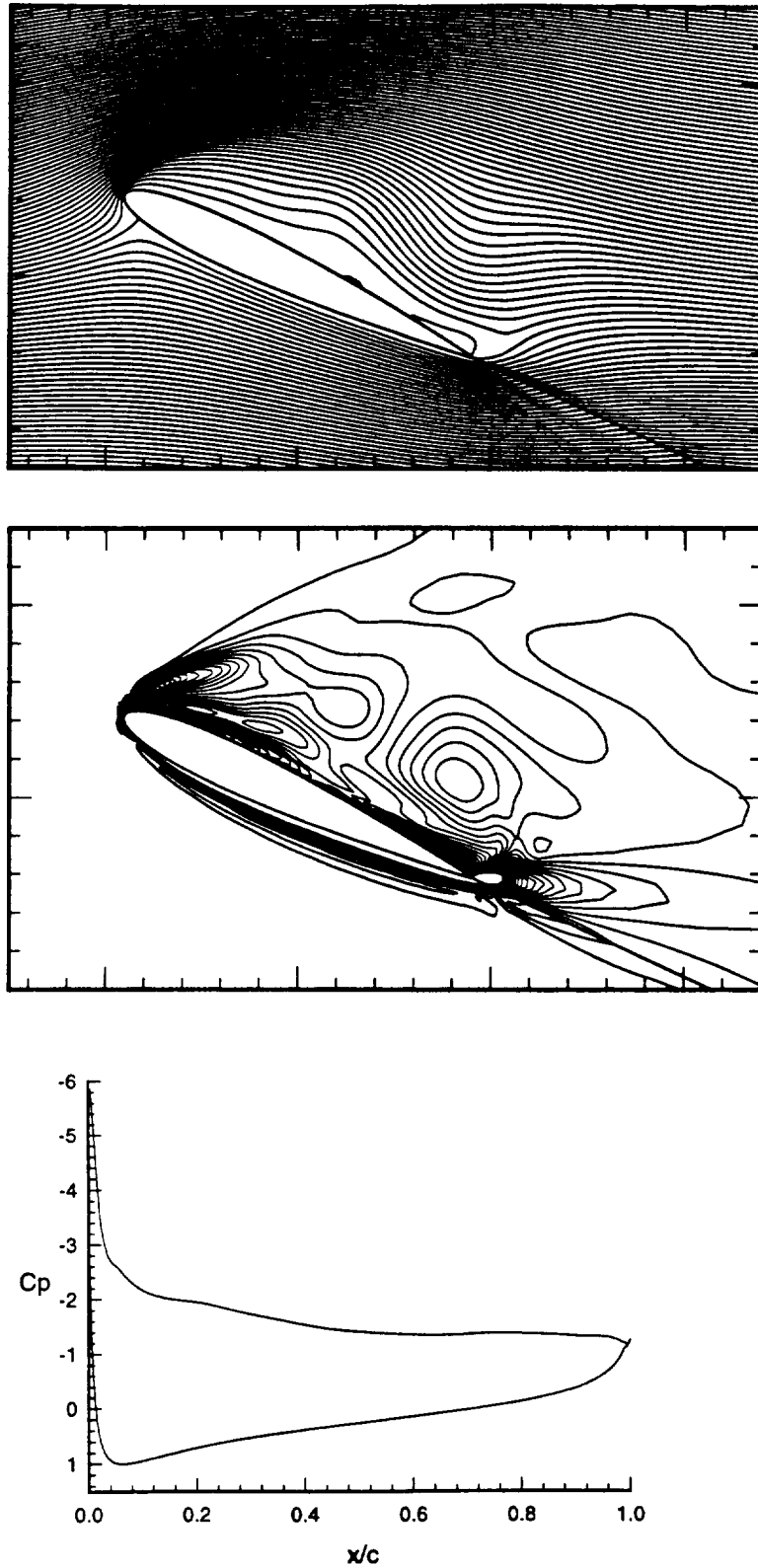
Figure 15. Time-averaged Streamlines (a), vorticity contours (b), and pressure coefficient (c) of NACA-0012 airfoil. The flow conditions are the same as that of Fig. 6.
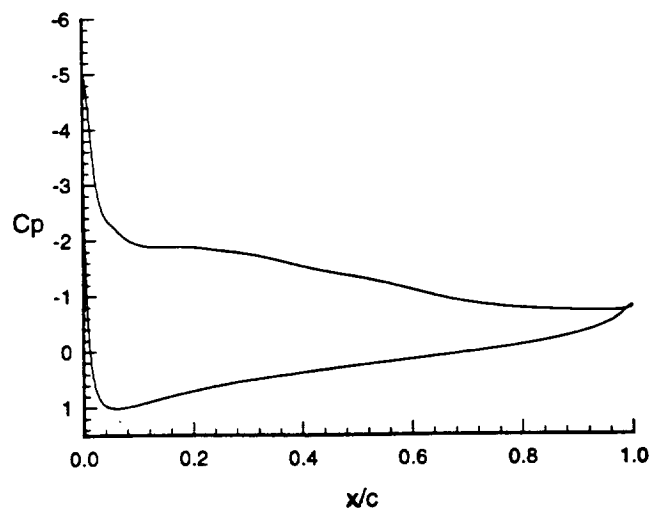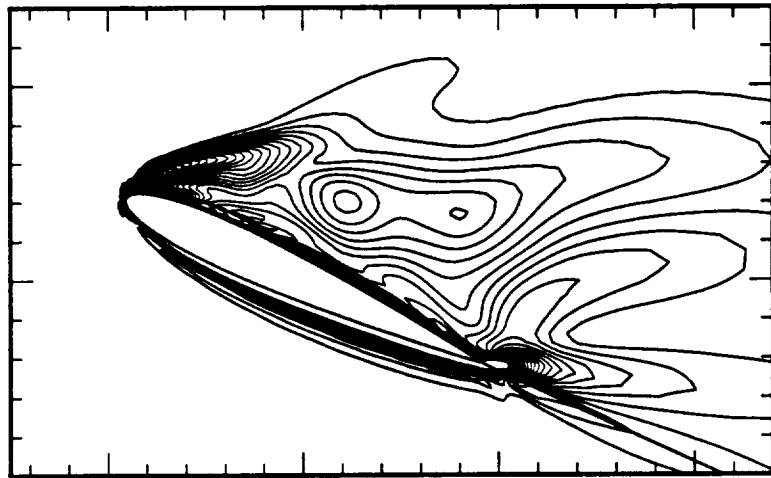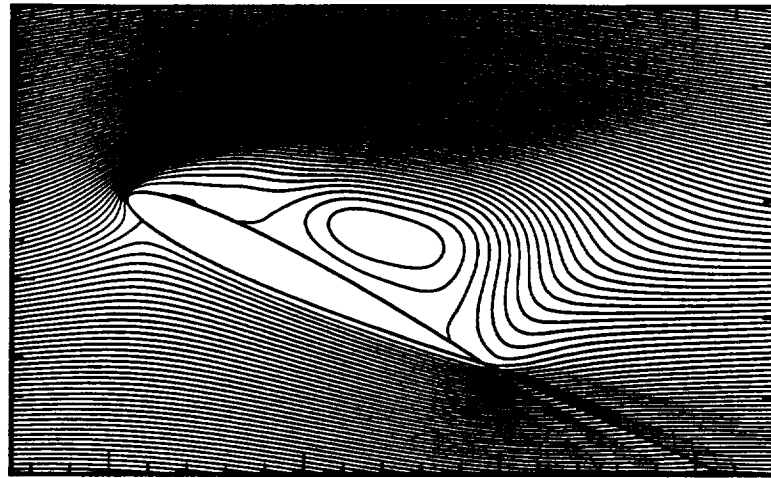
Figure 16. Time-averaged Streamlines (a), vorticity contours (b), and pressure coefficient (c) of NACA-0012 airfoil. The flow conditions are the same as that of Fig. 7.
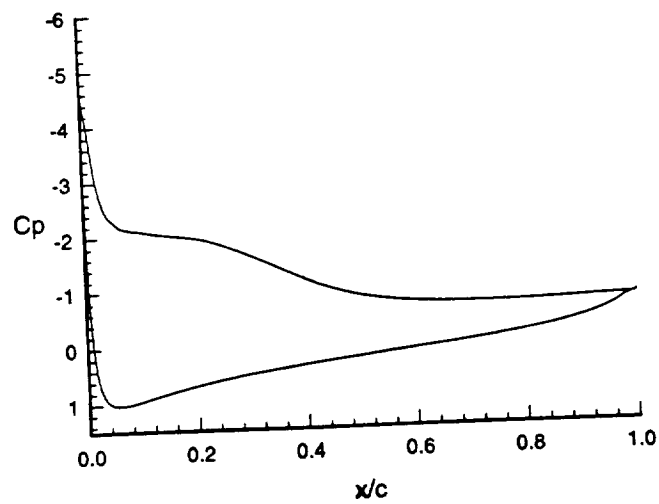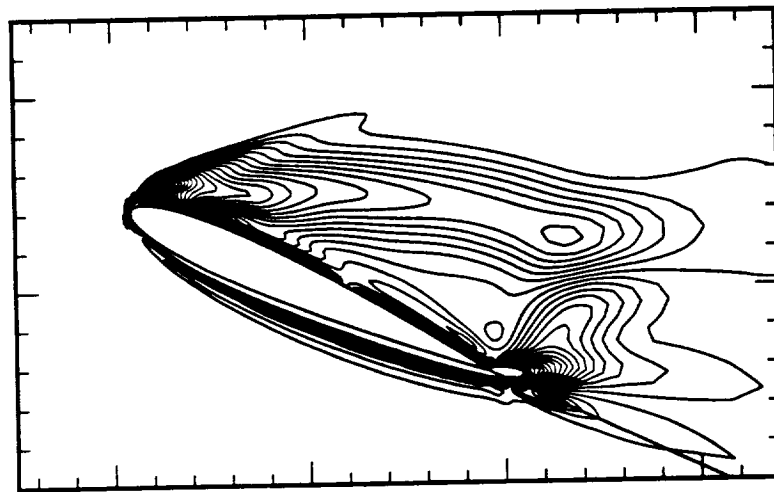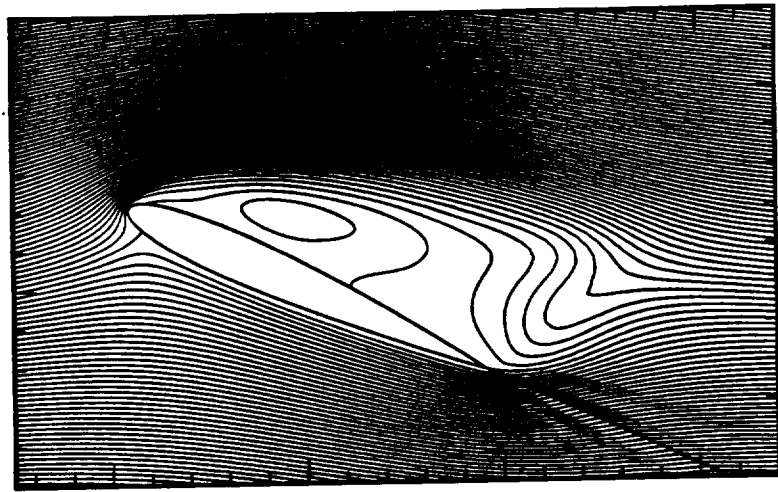
Figure 17. Time-averaged Streamlines (a), vorticity contours (b), and pressure coefficient (c) of NACA-0012 airfoil. The flow conditions are the same as that of Fig. 8.
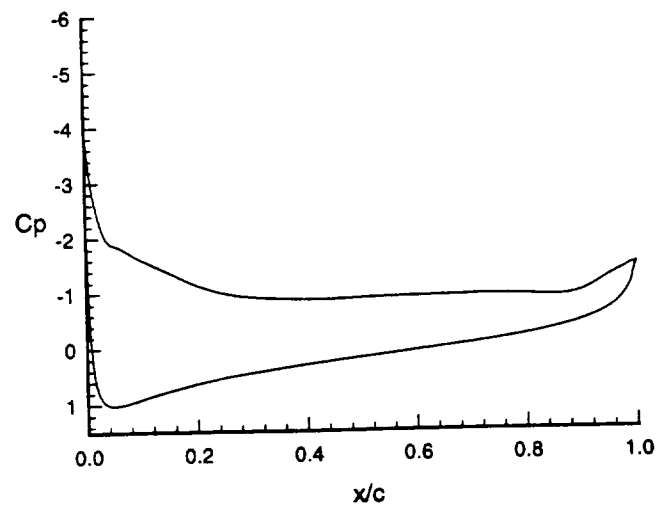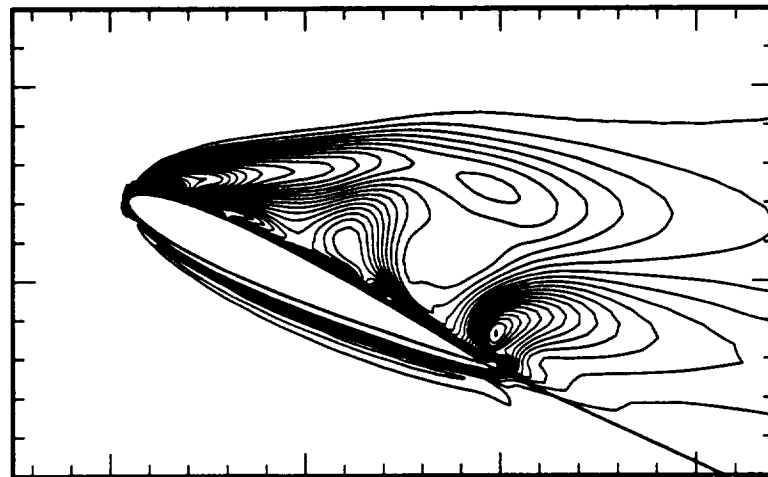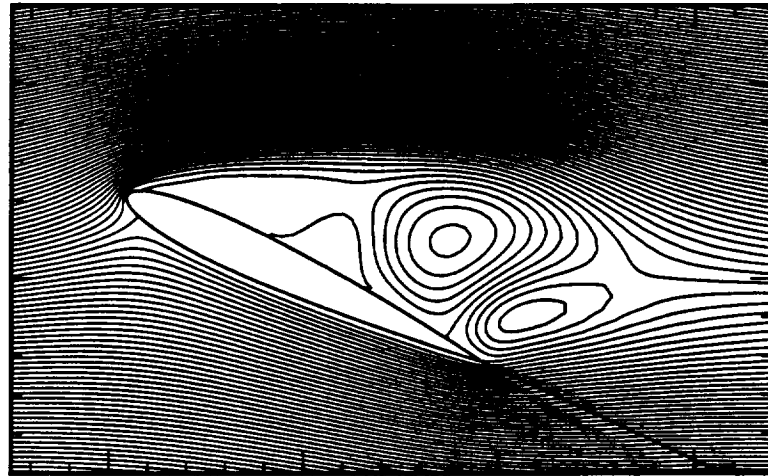
Figure 18. Time-averaged Streamlines (a), vorticity contours (b), and pressure coefficient (c) of NACA-0012 airfoil. The flow conditions are the same as that of Fig. 9.
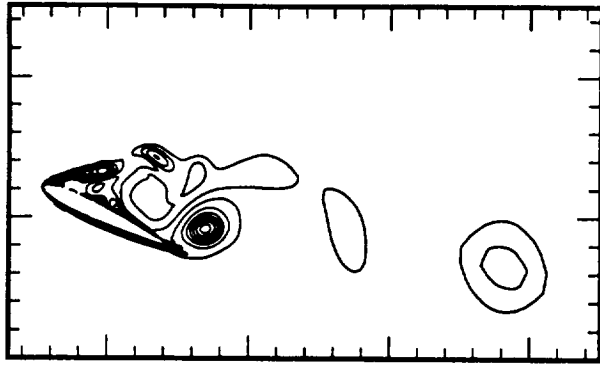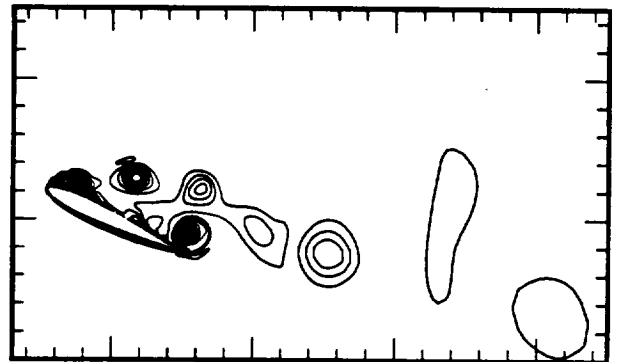
(g)
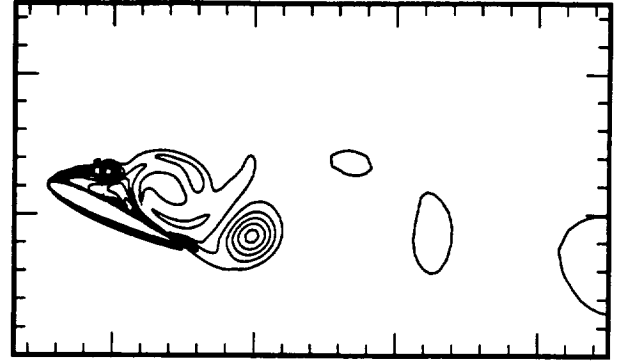
(h)
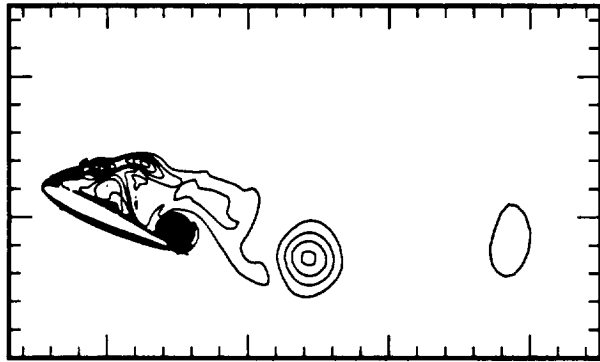
(i)
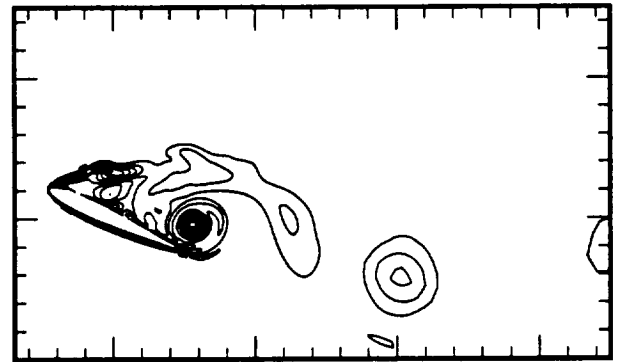
(j)

Figure 19. Instantaneous vorticity contours of NACA-0012 airfoil. Unforced flow, the same condition as Fig. 5. t = 113.07 (a); 113.77 (b); 114.47 (c); 115.17 (d); 115.87 (e); 116.58 (f); 117.28 (g); 117.98 (h); 118.68 (i); 119.38 (j).
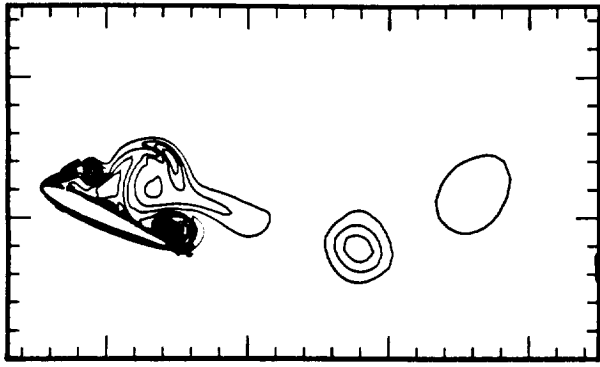
(a)
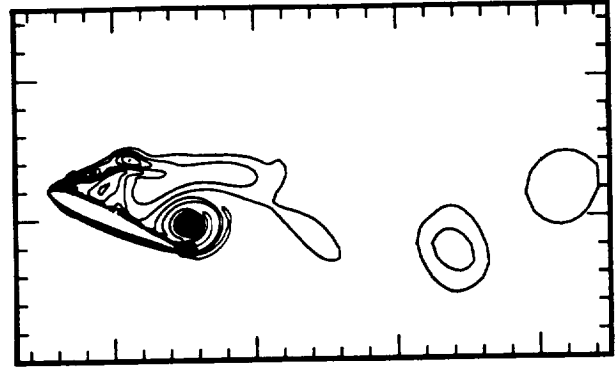
(b)
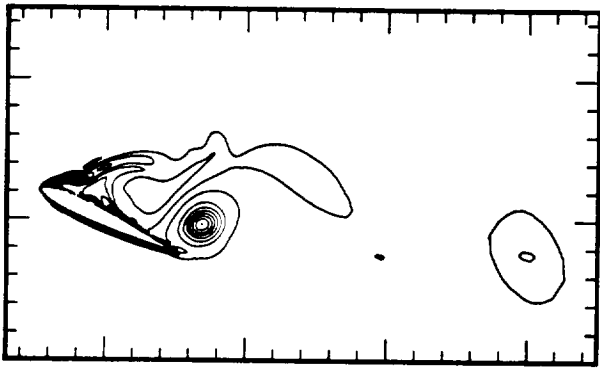
(c)
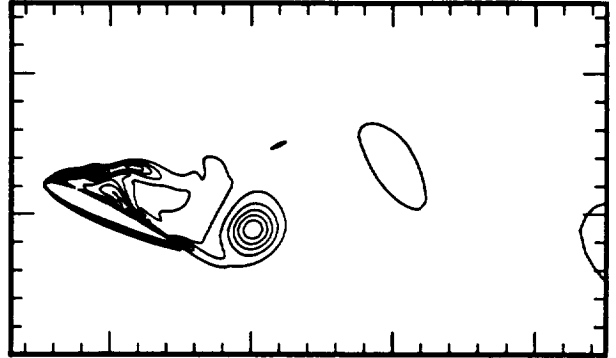
(d)
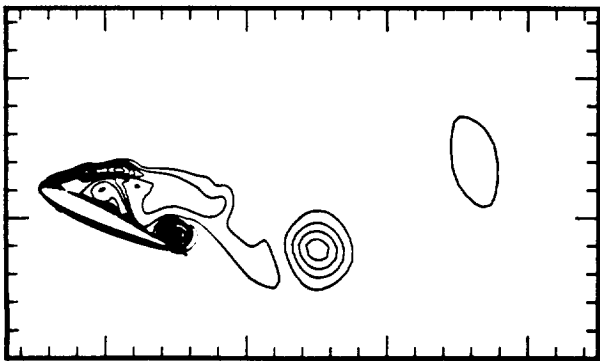
(e)
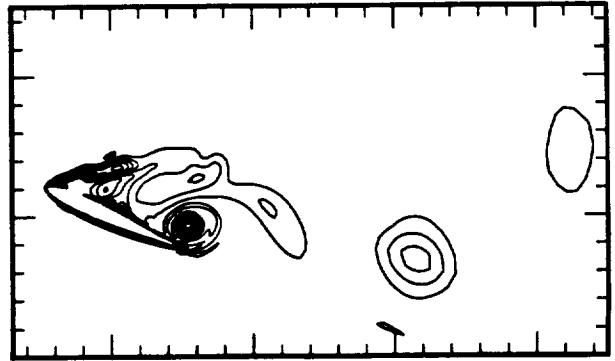
(f)

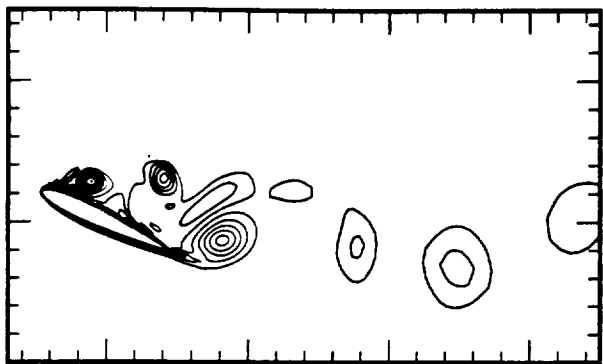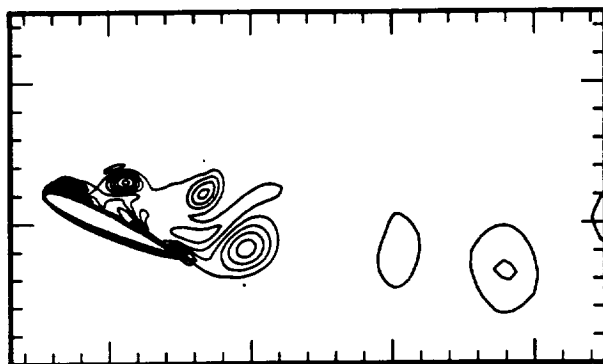Figure 19 (continued)
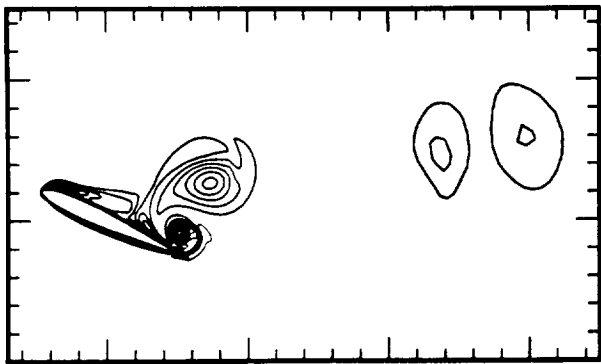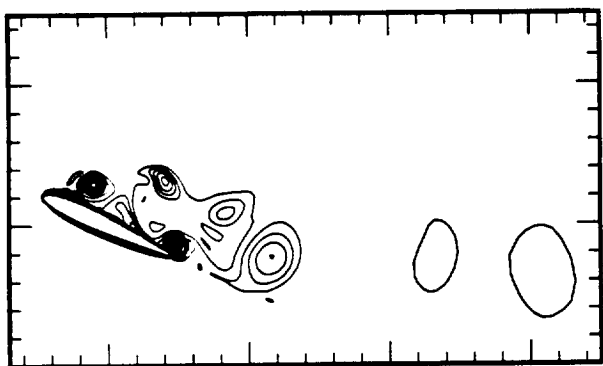
(g)
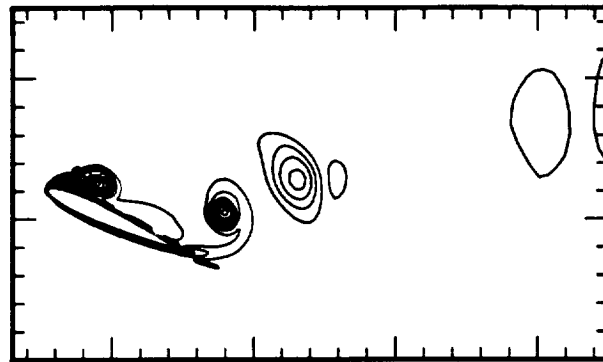
(h)
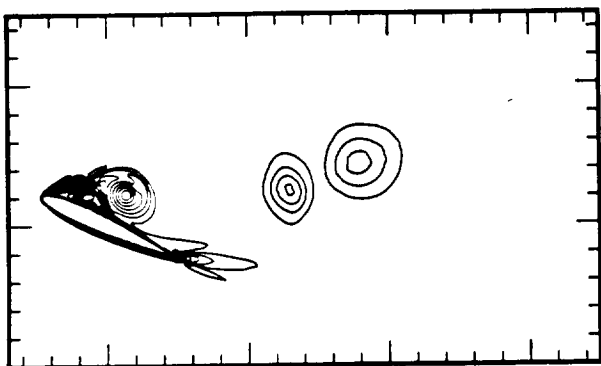
(i)
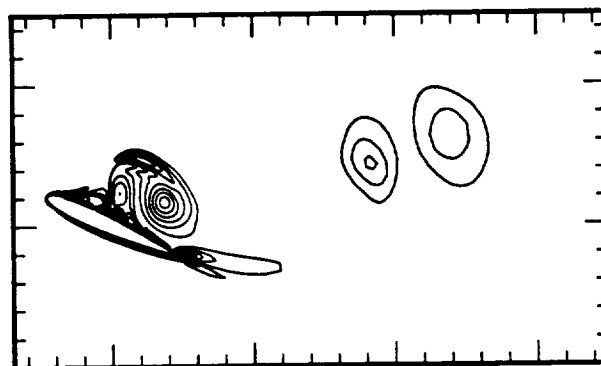
(j)

Figure 20. Instantaneous vorticity contours of NACA-0012 airfoil. Forced flow, the same condition as Fig. 7. $\widehat{f_e} = 1.0$. $t = 135.59$ (a); 136.29 (b); 136.99 (c); 137.69 (d); 138.39 (e); 139.09 (f); 139.79 (g); 140.49 (h); 141.19 (i); 141.89 (j).
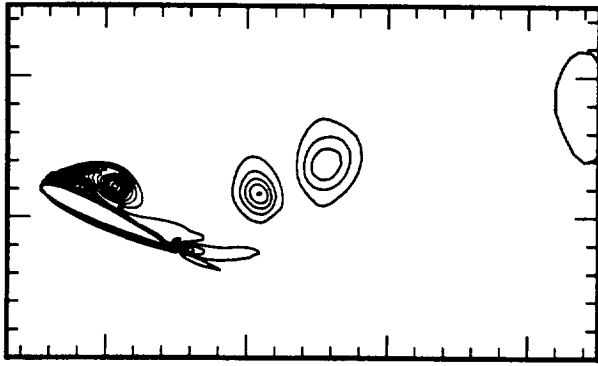
(a)
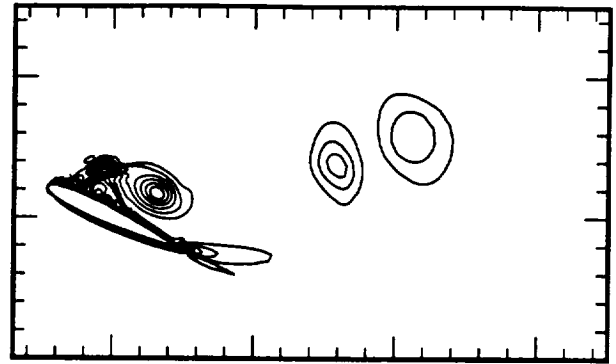
(b)
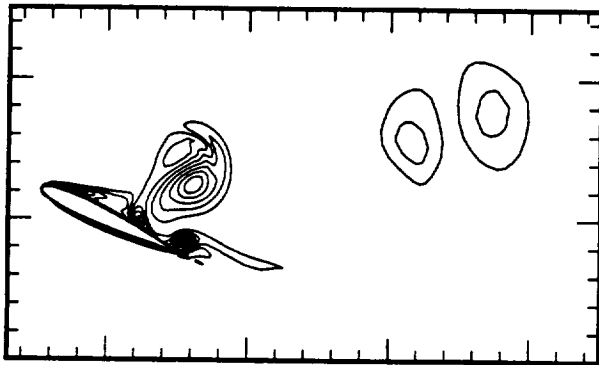
(c)
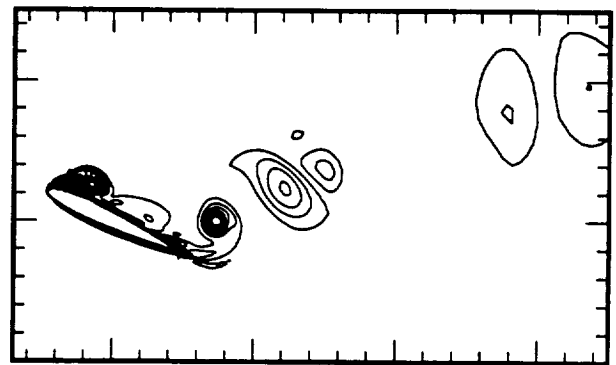
(d)
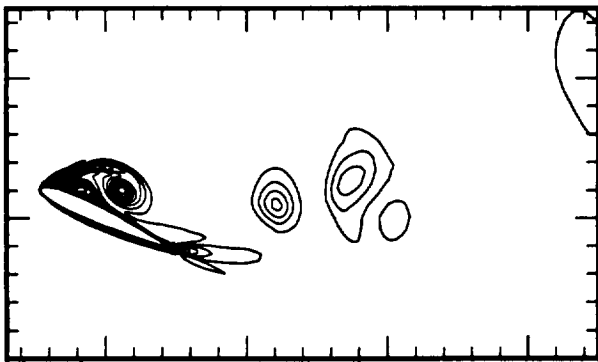
(e)
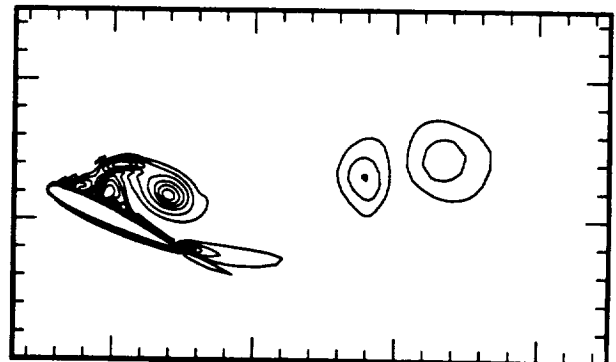
(f)

Figure 20 (continued)
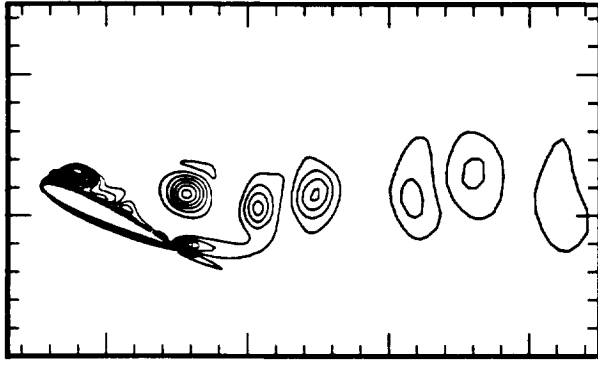
(g)
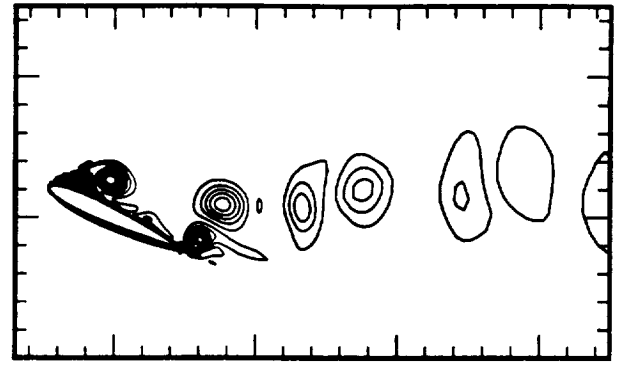
(h)
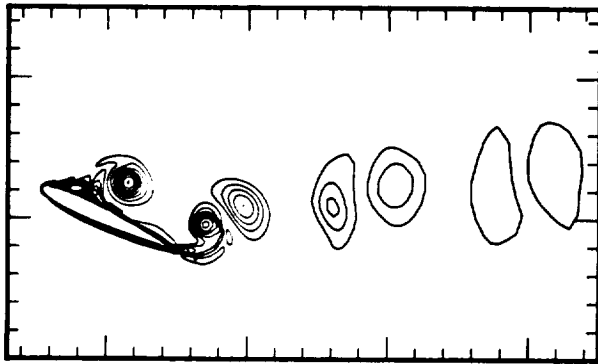
(i)
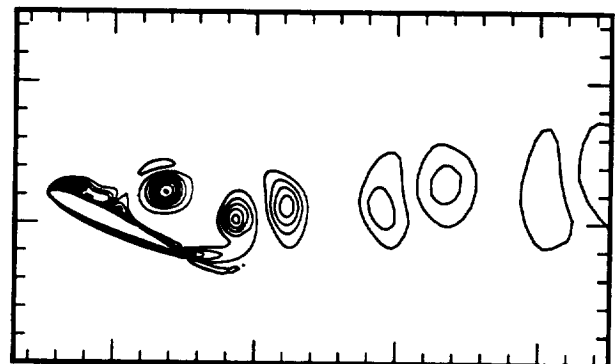
(j)

Figure 21. Instantaneous vorticity contours of NACA-0012 airfoil. Forced flow, the same condition as Fig. 8. $\widehat{f}_e = 2.0$. $t = 135.55$ (a); 135.89 (b); 136.23 (c); 136.57 (d); 136.91 (e); 137.24 (f); 137.58 (g); 137.92 (h); 138.26 (i); 138.60 (j).
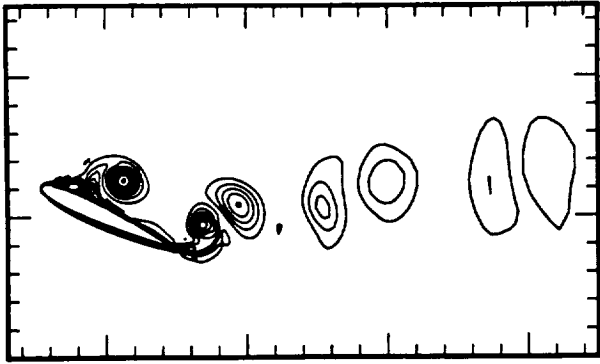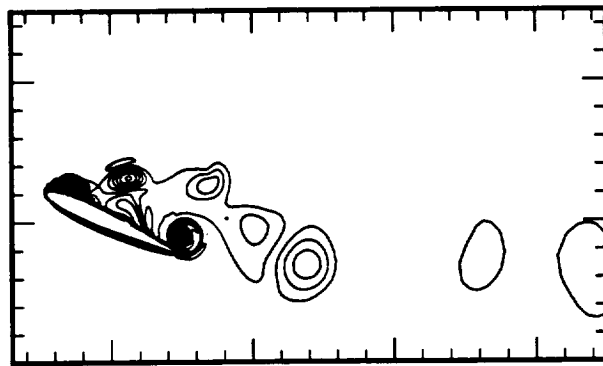
(a)
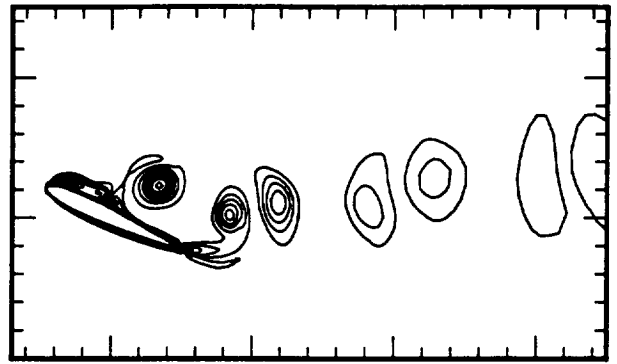
(b)
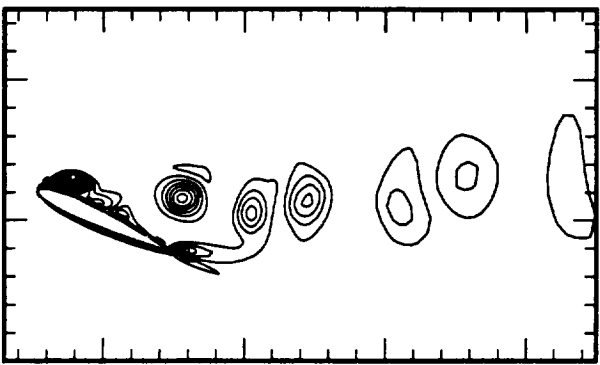
(c)
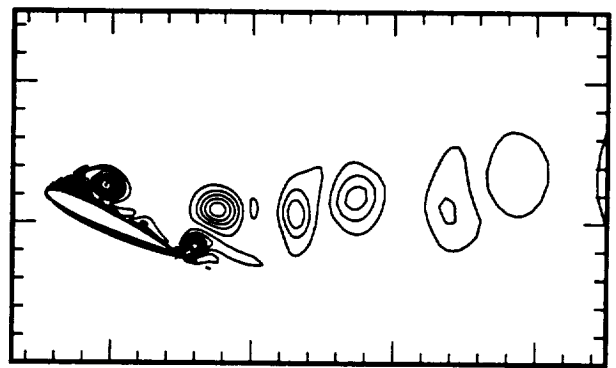
(d)
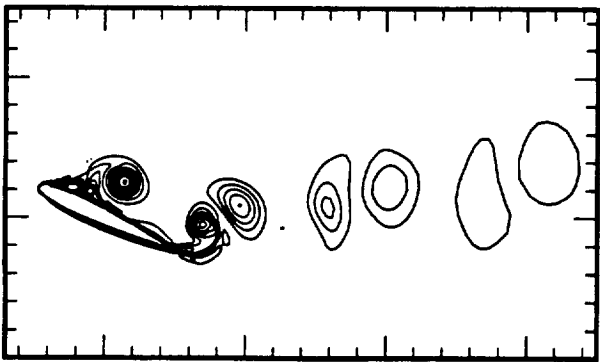
(e)
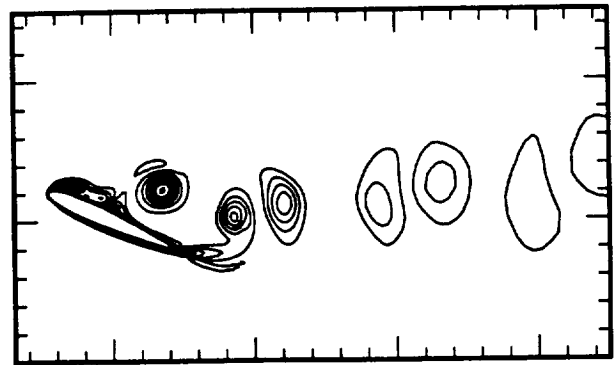
(f)

Figure 21 (continued)
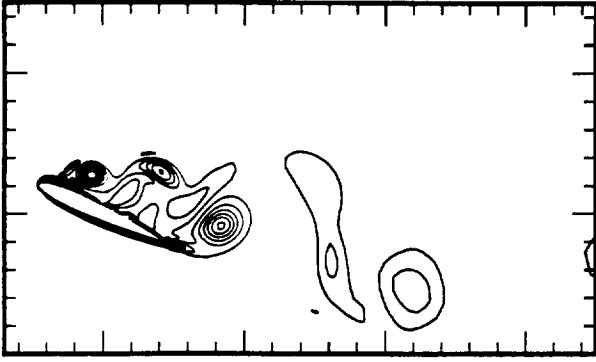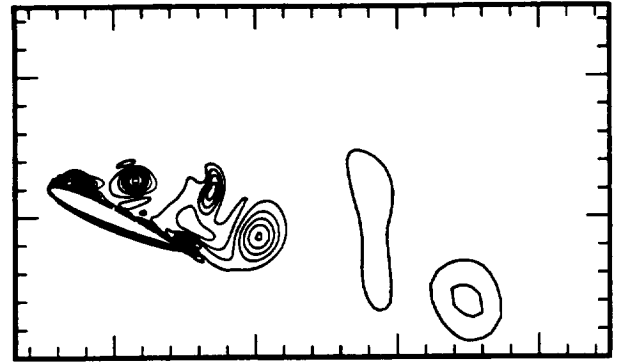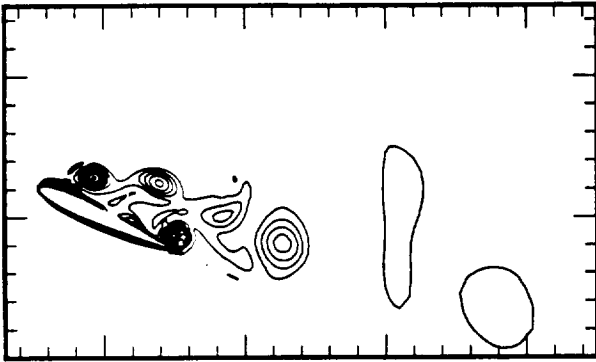
Figure 22. Instantaneous vorticity contours of NACA-0012 airfoil. Forced flow, the same condition as Fig. 9. $\widehat{f}_e = 4.0$. $t = 135.65$ (a); 135.99 (b); 136.33 (c); 136.67 (d); 137.00 (e); 137.34 (f); 137.68 (g); 138.02 (h); 138.36 (i); 138.70 (j).

(a)

(b)
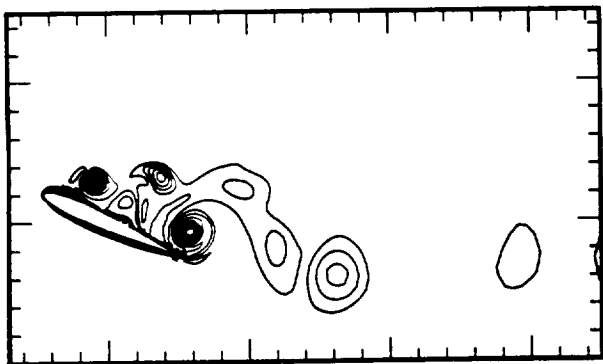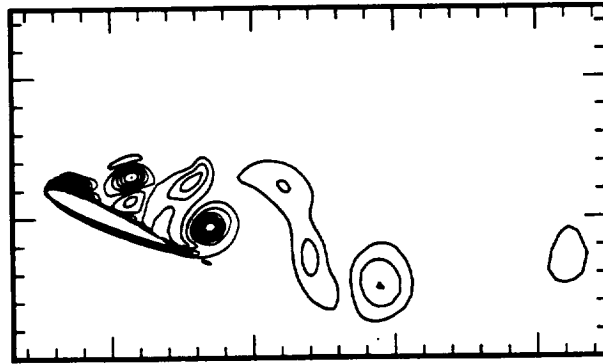
(c)

(d)

(e)

(f)

Figure 22 (continued)